Available online at www.sciencedirect.com
ScienceDirect
Geochimica et Cosmochimica Acta 75 (2011) 1642–1661
Geochimica et Cosmochimica Acta
www.elsevier.com/locate/gca

Using atmospheric fallout to date organic horizon layers and quantify metal dynamics during decomposition

James M. Kaste [a,*], Benjamin C. Bostick [b], Arjun M. Heimsath [c], Eiliv Steinnes [d], Andrew J. Friedland [e]

[a] Geology Department, The College of William & Mary, Williamsburg, VA 23187, USA
[b] Lamont-Doherty Earth Observatory of Columbia University, Route 9W, Palisades, NY 10964, USA
[c] School of Earth and Space Exploration, Arizona State University, Tempe, AZ 85287, USA
[d] Department of Chemistry, Norwegian University of Science and Technology, NO-7491 Trondheim, Norway
[e] Environmental Studies Program, Dartmouth College, Hanover, NH 03755, USA

Received 14 June 2010; accepted in revised form 5 January 2011; available online 14 January 2011

Abstract

High concentrations of metals in organic matter can inhibit decomposition and limit nutrient availability in ecosystems, but the long-term fate of metals bound to forest litter is poorly understood. Controlled experiments indicate that during the first few years of litter decay, Al, Fe, Pb, and other metals that form stable complexes with organic matter are naturally enriched by several hundred percent as carbon is oxidized. The transformation of fresh litter to humus takes decades, however, such that current datasets describing the accumulation and release of metals in decomposing organic matter are timescale limited. Here we use atmospheric ^{210}Pb to quantify the fate of metals in canopy-derived litter during burial and decay in coniferous forests in New England and Norway where decomposition rates are slow and physical soil mixing is minimal. We measure ^{210}Pb inventories in the O horizon and mineral soil and calculate a 60–630 year timescale for the production of mobile organo-metallic colloids from the decomposition of fresh forest detritus. This production rate is slowest at our highest elevation (~1000 m) and highest latitude sites (>63°N) where decomposition rates are expected to be low.

We calculate soil layer ages by assuming a constant supply of atmospheric ^{210}Pb and find that they are consistent with the distribution of geochemical tracers from weapons fallout, air pollution, and a direct ^{207}Pb application at one site. By quantifying a gradient of organic matter ages with depth in the O horizon, we describe the accumulation and loss of metals in the soil profile as organic matter transforms from fresh litter to humus. While decomposition experiments predict that Al and Fe concentrations increase during the initial few years of decay, we show here that these metals continue to accumulate in humus for decades, and that enrichment occurs at a rate higher than can be explained by quantitative retention during decomposition alone. Acid extractable Al and Fe concentrations are higher in the humus layer of the O horizon than in the mineral soil immediately beneath this layer: it is therefore unlikely that physical soil mixing introduces significant Al and Fe to humus. This continuous enrichment of Al and Fe over time may best be explained by the recent suggestion that metals are mined from deeper horizons and brought into the O horizon via mycorrhizal plants. In sharp contrast to Al and Fe, we find that Mn concentrations in decomposing litter layers decrease exponentially with age, presumably because of leaching or rapid uptake, which may explain the low levels of acid extractable Mn in the mineral soil. This study quantifies how metals are enriched and lost in decomposing organic matter over a longer timescale than previous studies have been able to characterize. We also put new limits on the rate at which metals in litter become mobile organo-metallic complexes that can migrate to deeper soil horizons or surface waters.
© 2011 Elsevier Ltd. All rights reserved.

1. INTRODUCTION

High concentrations of trace (e.g., Pb, Cu, Cd, Hg) and major (e.g., Al, Fe) metals in organic matter can inhibit

* Corresponding author. Tel.: +1 757 221 2951.
E-mail address: jmkaste@wm.edu (J.M. Kaste).

0016-7037/$ - see front matter © 2011 Elsevier Ltd. All rights reserved.
doi:10.1016/j.gca.2011.01.011

microbial processes responsible for decomposition and directly limit nutrient availability in soils (Brynhildsen and Rosswall, 1997; Giesler et al., 2002; Chaperon and Sauve, 2007). The organic (O) horizons of temperate and boreal forests that comprise nearly 70% of the world's terrestrial surface detritus (Schlesinger, 1977) receive high loadings of metals from anthropogenic and natural processes (Galloway et al., 1982; Berg et al., 1994). Organic matter decomposition regulates the cycling of nutrients in ecosystems, influences the amount of carbon in the atmosphere, and plays an important role in chemical weathering processes (Drever, 1992; Davidson and Janssens, 2006). Despite the impact that metals can have on biogeochemical processes in the O horizon, and the potential of these layers to be a long-term source of metals to deeper soil horizons and surface waters, we lack a quantitative understanding of how metals behave in decomposing terrestrial organic matter (Brandtberg and Simonsson, 2003; Li et al., 2008).

After metals are delivered to the soil surface by litterfall, atmospheric deposition, and root uptake, the speciation, residence time, and ultimate fate of these elements have been difficult to describe. Litterbag experiments have shown that the Al and Fe content of organic matter increases with decomposition as mass is lost via oxidation and stable complexes are formed presumably between the metals and organic matter functional groups (Rustad, 1994). Other elements such as Ca and P decrease dramatically in decomposing litter from either leaching or recirculation. The decomposition of organic matter may drive fundamental shifts in metal speciation on timescales of just a few years (Schroth et al., 2008). Although useful, decomposition experiments only provide us with a short (<5 years) window of observation on the behavior of metals during organic matter decay; we lack a method for evaluating the long-term fate of elements that accumulate in more recalcitrant organic matter that could be stable for decades.

Natural and anthropogenic radioactive fallout from the atmosphere are used extensively to date peat and sedimentary deposits (Appleby, 2008) and to quantify short-term (<100 years) transport processes in fluvial, shallow shelf and deep marine environments (Robbins et al., 1977; Bonniwell et al., 1996; Wallbrink et al., 1999). Atmospherically-deposited ^{210}Pb, weapons-derived ^{241}Am and ^{207}Bi, and cosmogenic ^{7}Be have a strong affinity for organic matter functional groups (Kim et al., 1997; Sauve et al., 2000; Artinger et al., 2002). These tracers along with other pollutants offer a potentially powerful tool for studying poorly understood biogeochemical processes on the short but extremely pertinent timescale of 1–100 years (Kaste et al., 2007; Klaminder and Yoo, 2008; Dixon et al., 2009). To date, however, their use in soil environments has been limited, presumably because of potential complications with preferential flow paths and physical mixing that would complicate steady-state and initial condition assumptions necessary for absolute dating models.

Here we apply natural and pollutant atmospheric fallout to trace canopy-derived litter in well-drained forested soil profiles where physical soil mixing rates are relatively low. We use cosmogenic ^{7}Be ($T_{1/2} = 53$ days) to constrain the maximum depth to which particle-reactive atoms penetrate in soil during intense precipitation events, and test a constant rate of supply (CRS) ^{210}Pb ($T_{1/2} = 22$ years) model for dating O horizon layers using depth-profiles of pollutant Pb, weapons fallout radionuclides ^{241}Am and ^{207}Bi, and a direct ^{207}Pb application at one site. We use high-resolution concentration-depth distributions of metals and radionuclides in the whole profile to evaluate sources of elements to the O horizon. Using CRS ^{210}Pb chronology we quantify the enrichment and loss of Al, Fe, and Mn in organic matter as freshly deposited forest detritus is buried and decomposes to humus over the timescale of 1–100 years. Our work shows how organic matter can naturally accumulate Fe and Al for decades through both decomposition and below-ground circulation. In contrast, our results suggest that biological demand and/or dissolved transport can strip Mn from decomposing litter over the course of just a few years. Our steady-state ^{210}Pb transport model puts new limits on the rate at which strongly hydrolyzing metals in litter can become mobile organo-metallic complexes that migrate to deeper soil horizons or possibly to surface waters.

2. METHODS

2.1. Site locations and sampling description

Field sites were selected to span a range of variables that could potentially control organic matter decomposition and metal dynamics, including elevation, latitude, and canopy type (Berg, 2000; Schroth et al., 2008). We quantitatively sampled the soil profiles of several Spodosols in undisturbed areas throughout Norway and in Vermont, New Hampshire and Maine, USA to measure the vertical distribution of organic matter, metals, and fallout nuclides (Table 1). These regions were recently glaciated and the soils at our sites are acidic, developing primarily on till dominated by silicate minerals. We only sampled on gentle slopes and used maps and field observations to avoid areas that had been logged or developed in recent decades, and the three sites in the US are on protected land. The presence of sharp and distinct soil horizons, particularly between the O horizon and the mineral soil indicates that the biogeochemical processes of decomposition and leaching outpace physical soil mixing from organisms or freeze–thaw cycles (Kaste et al., 2007). Soils in our sampling areas are sandy and very well drained, having clear eluviation and illuviation horizons in the weathering profile, and appear to be neither eroding or aggrading on short (decades) timescales. We specifically chose sites where there was no evidence of groundwater upwelling or emergence in any of the profiles, such that we assume that water flows from the surface downwards rather than laterally or upwards.

At each profile, we extracted a sample of the entire ~8–12-cm O horizon by cutting around and beneath a 15 cm × 15 cm wooden template which we subsequently sliced into ~1–2 cm sections with a stainless-steel knife. All live vegetation, organic matter, and roots that were in the layer or crossed the layer were cut and included with the sample. At least three bulk (not sectioned) O horizons were extracted to evaluate variability in the O horizon mass at each site (σ = standard deviation in Table 1). After the O

Table 1
Sampling locations. Range given for O horizon mass and OM content is 2σ. Sites are described in more detail elsewhere in Miller and Friedland (1994), Kaste et al. (2003), Donisa et al. (2005), Steinnes et al. (2005), and Kaste et al. (2007). Sites 1 and 2 are at relatively high elevation (~1000 m) compared with the other sites (<250 m), but all soils were sampled on gentle (<15 degree slopes) as described in Section 2.

Site	Lat/long	Elevation (m)	Vegetation	O horizon mass (kg m^{-2})
1.Camels Hump, VT	44°19′N; 72°53′W	975	Red Spruce/Balsam Fir/Yellow Birch	10–15
2. Moosilauke, NH	44°0′N; 71°50′W	960	Red Spruce/Yellow Birch/Hemlock	9–14
3. Ducktrap, ME	44°16′N; 69°1′W	40	Spruce/Birch/Hemlock Mix	6–8
4. Mosvik, Norway	63°48′N; 10°49′E	230	Norway Spruce	6–8
5. Evje, Norway	58°32′N; 7°44′E	190	Scots Pine	6–7
6. Birkenes, Norway	58°22′N; 8°15′E	120	Norway Spruce	6–8
7. Amli, Norway	58°42′N; 8°21′E	180	Scots Pine	5–7

horizon was removed, we excavated a pit to approximately 1 m, and pressed acid-washed plastic centrifuge tubes (50 ml) into a cleaned face. We sampled mineral soil in triplicate every 4 cm from the base of the O horizon down to the C horizon.

2.2. Radionuclide measurements

We used high-purity intrinsic Ge detectors (Canberra Broad Energy) with ultra-low background hardware and copper-lined lead shields to measure radionuclide concentrations in soil samples. Organic and mineral soil samples were air dried and packed into plastic containers for gamma analysis. We determined detector efficiency for U-series radionuclides in different counting geometries using certified uranium ore (Canadian Certified Reference Materials Project BL-5 U ore) and used a mixed radionuclide solution (Isotope Products) for efficiency calibration at other energies. Corrections are made for self-attenuation of the 46 keV ^{210}Pb photon using standard techniques (Cutshall et al., 1983), and the 186 keV ^{226}Ra line was corrected for the ^{235}U interference by simultaneously measuring the uranium content of the sample at 63 keV (Dowdall et al., 2004; Kaste et al., 2006b). Samples were measured for weapons-derived fallout radionuclides ^{241}Am and ^{207}Bi by quantifying their gamma emissions at 59.5 and 569.7 keV, respectively, and cosmogenic ^{7}Be was measured via its 477.6 keV gamma emission. Radionuclide data are reported in units of concentration per mass (Bq kg^{-1}) and amounts per area (Bq m^{-2}) using the bulk density measurements of each horizon. Typical one-sigma analytical errors for the ^{210}Pb and ^{226}Ra activity determinations are 3% and 6%, respectively, and 5–10% for ^{7}Be and the weapons-derived nuclides (depending on actual counts collected). In Table 2, $^{210}Pb_{ex}$ inventory uncertainties are determined by propagating the actual one-sigma counting errors on the ^{210}Pb and ^{226}Ra analyses and a conservative estimate of 10% uncertainty on the bulk density measurements. Further details on our treatment of the uncertainties are given below and in the Appendix.

In order to estimate the contribution of mineral-derived elements in O horizon layers, we quantify Th in samples by simultaneously measuring its granddaughter radioisotopes ^{212}Pb (239 keV), ^{208}Tl (583 keV), and ^{228}Ac (911 keV). Detector efficiency for these nuclides was calculated using a Thorium standard reference material (Canadian Certified Reference Materials Project Dl-1a). Because the use of ^{232}Th series isotopes to measure total Th assumes radioactive equilibrium, we re-measured Th on a subset of samples after 5 years of storage in a closed-system. Changes in activity of the ^{232}Th series nuclides would be measurable over this timeframe if disequilibrium were significant, since the longest half-life of the nuclides beneath ^{232}Th is 5.8 years (^{228}Ra). However, measured activities of the ^{232}Th series nuclides before and after storage were not appreciable (<15%), so we maintain that the use of these short-lived daughter isotopes to quantify relative changes of Th within a soil profile is reasonable. Detection limits for Th using this technique are a function of the time counted, mass counted, and variability of the Compton background near the photopeak energies for ^{212}Pb, ^{228}Ra, and ^{228}Ac. Given our typical counting configuration of 16 g of soil counted for 100 ks, 3σ of the background gives a detection limit of ~0.2 mg kg^{-1} Th.

2.3. Determination of organic matter content and acid-extractable metals

In the laboratory, we air-dried and weighed the samples, and calculated soil dry bulk density by dividing the mass collected by the volume extracted. We utilized a hot nitric acid extraction to quantify an operationally-defined "labile" metal content, which would be the metals that are incorporated in organic matter and associated with secondary mineral phases. Nitric-acid extractable (NAE, hereafter) metals are determined by ashing 2 g of oven-dried (105 °C) soil at 475 °C for 8 h, and mass loss on ignition during this process was used to calculate percent organic matter (OM). After ignition, the ash is dissolved in boiling 8 M HNO_3 (1 part H_2O, 1 part concentrated nitric acid) for 20 min in a 30 ml silica crucible. Extracts are filtered (Whatman #41) and diluted to 50 ml with deionized water. Major (Al, Ca, Fe, K, Mg, Mn, Na) and trace elements (Cd, Cu, Pb, Zn) are measured on the dilute extracts using ICP-OES. Recoveries of Al, Fe, Mn, and Pb from a Pine Needles reference material (High Purity Standards) were always within 15% of the certified values using this method. Concentrations of NAE Al, Fe, Mn, and Pb are expressed in amount metal per air-dry mass soil (mg kg^{-1}).

2.4. Recovery of an enriched ^{207}Pb tracer application

We use the results of a previous study (Kaste et al., 2003) as an independent check on the ^{210}Pb dating model

Table 2
Density, organic matter content (%OM measured by percent mass loss on ignition of an oven-dried sample), NAE Pb, $^{210}Pb_{ex}$, and ^{241}Am measurements in soil layers. CRS ages and uncertainties are calculated by propagating the measurement errors in the $^{210}Pb_{ex}$ inventories and are relative to the sampling year (see Appendix for details on uncertainty determination). ^{241}Am detection limits (uncertainty) is typically 0.4 Bq kg^{-1} and 2 mg kg^{-1} for NAE Pb. ^{210}Pb measurements for Sites 1 and 2 were made during previous studies ([†]Kaste et al., 2003 and [‡]Kaste et al., 2007).

Depth increment (cm)	Horizon	Thickness (cm)	Density (g cm^{-3})	OM (%)	NAE Pb (mg kg^{-1})	^{241}Am (Bq kg^{-1})	$^{210}Pb_{ex}$ (Bq kg^{-1})	^{241}Am (Bq m^{-2})	$^{210}Pb_{ex}$ (Bq m^{-2})	CRS age	σ_t
Camels Hump, VT[†]											
0–4	Oi	4	0.07	95	42	nd	980	nd	2744 ± 271	1995–2001	<1
4–8	Oe	4	0.13	93	155	0.9	1035	4.7	5382 ± 540	1979–1995	1
8–12	Oa	4	0.15	90	252	5.2	770	31	4620 ± 461	1952–1979	2
12–17	Oa	5	0.21	81	72	1.9	260	20	2730 ± 273	1904–1952	3
17–19	B	2	0.53	22	25	nd	75	nd	795 ± 127	<1904	4
19–21	B	2	0.64	17	11	nd	nd	nd	Nd		
Ducktrap, ME											
0–1	Oi	1	0.08	97.6	2.7	nd	354	nd	282 ± 28	2005–2006	<1
1–2.5	Oe	1.5	0.08	96.0	11.2	nd	751	nd	891 ± 89	2000–2005	1
2.5–4	Oe	1.5	0.09	95.9	17.2	nd	743	nd	964 ± 96	1995–2000	1
4–6	Oa	2	0.08	95.5	45.4	0.39	709	1	1156 ± 116	1987–1995	1
6–8	Oa	2	0.10	92.3	105.6	3	544	6	1044 ± 104	1977–1987	2
8–10	Oa	2	0.12	76.9	92.2	3.2	343	8	850 ± 85	1967–1977	3
10–13	B	3	0.58	14.3	20.9	0.5	76.5	9	1337 ± 214	<1967	4
13–17	B	4	0.67	10.3	14.6	0.4	23	11	616 ± 98		
17–20	B	4	0.90	12.1	7.8	nd	6		216 ± 97		
Moosilauke, NH[‡]											
0–1	Oi	1	0.07	96.8	8.0	nd	677		474 ± 47	2002–2004	<1
1–4.5	Oe	3.5	0.08	95.7	61.9	1.2	842	3	2358 ± 236	1992–2002	1
4.5–6.5	Oa	2	0.14	93.0	134.8	3	850	8	2380 ± 238	1976–1992	1
6.5–9	Oa	2.5	0.14	87.3	203.6	6	482	21	1687 ± 169	1958–1976	2
9–11	Oa	2	0.16	76.5	111.4	2.9	240	9	768 ± 77	1944–1958	3
11–13.5	E	2.5	0.62	10.5	95.8	nd	75	0	1163 ± 186	<1944	3
13.5–16	E	2.5	0.58	3.9	13.1	nd	12	0	174 ± 33		
16–18	E	2	0.72	4.5	5.8	nd	0		0		
18–20	Bh	2	0.65	19.8	7.4	nd	5		65 ± 29		
Evje, Norway											
0–1	Oi	1	0.06	97.9	14.1	nd	560	nd	363 ± 35	2000–2004	<1
1–3	Oe	2	0.05	97.6	30.1	nd	699	nd	711 ± 71	1991–2000	1

(*continued on next page*)

Table 2 (*continued*)

Depth increment (cm)	Horizon	Thickness (cm)	Density (g cm^{-3})	OM (%)	NAE Pb (mg kg^{-1})	^{241}Am (Bq kg^{-1})	$^{210}Pb_{ex}$ (Bq kg^{-1})	^{241}Am (Bq m^{-2})	$^{210}Pb_{ex}$ (Bq m^{-2})	CRS age	σ_t
3–4.5	Oa	1.5	0.10	96.0	166.7	1.24	520	2	802 ± 80	1976–1991	2
4.5–7	Oa	2.5	0.12	77.9	1040.9	6.58	346	19	1003 ± 100	1934–1976	2
7–10	A	3	0.40	19.6	64.5	nd	31	nd	372 ± 60	<1934	3
10–14	E	4	0.70	1.8	4.5	nd	nd	nd	nd		
14–18	B	4	0.80	9.5	28.9	nd	nd	nd	nd		
Amli, Norway											
0–1.5	Oi	1.5	0.06	97.7	8.8	0	521	0	489 ± 48	2002–2004	<1
1.5–3	Oe	1.5	0.06	97.6	34.0	0	751	0	708 ± 70	1998–2002	1
3–4	Oe	1	0.14	88.6	59.4	1	781	1	1097 ± 109	1991–1998	1
4–5	Oe	1	0.19	93.8	136.5	1.7	558	3	1052 ± 105	1983–1991	1
5–7	Oa	2	0.13	88.8	135.5	4.35	402	12	1077 ± 107	1971–1983	2
7–8.5	A	1.5	0.35	26.6	76.9	1.75	119	9	627 ± 64	<1971	3
8.5–12.5	Bs	4	0.70	11.0	41.1	1.6	60	45	1680 ± 269		
12.5–16.5	Bs	4	0.90	5.4	22.8	0	6	0	216 ± 99		
16.5–20	Bs	3	0.90	5.5	9.4	0	0	0	0		
Birkenes, Norway											
0–1.25	Oi	1.25	0.06	95.0	26.2	nd	1274	nd	987 ± 98	1998–2004	<1
1.25–2.5	Oe	1.25	0.07	94.0	83.6	nd	1183	nd	990 ± 99	1990–1998	1
2.5–4	Oe	1.5	0.08	90.0	205.6	nd	1076	nd	1348 ± 133	1976–1990	2
4–5.5	Oa	1.5	0.09	78.0	241.2	4.04	561	5	743 ± 74	1965–1976	2
5.5–6.5	Oa	1	0.26	58.0	147.4	2.87	236	8	625 ± 62	1950–1965	3
6.5–8	A	1.5	0.33	34.0	82.2	1.4	66	7	324 ± 52	<1950	4
8–10	A2	2	0.65	15.0	70.5	0.1	50	1	650 ± 104		
10–15	E	5	0.85	2.0	17.4	nd	2	nd	85 ± 43		
15–18	E/B	3	0.85	3.0	23.2	nd	nd	nd	0		
Mosvik, Norway											
0–1.5	Oi	1.5	0.06	96.8	1.9	nd	580	nd	516 ± 51	1999–2004	<1
1.5–2.75	Oe	1.25	0.13	96.8	8.2	nd	583	nd	939 ± 83	1987–1999	1
2.75–3.75	Oe	1	0.14	95.9	24.4	2	468	3	636 ± 64	1975–1987	2
3.75–5.25	Oa	1.25	0.16	95.4	21.8	5.5	344	11	696 ± 70	1954–1975	2
5.25–6.0	Oa	0.75	0.16	91.3	20.5	4.43	225	5	268 ± 27	1940–1954	3
6–7.1	Oa	1.1	0.28	59.0	19.4	nd	92	nd	283 ± 37	1912–1940	4
7.1–11	A	3.9	0.4	20.4	13.7	nd	13	nd	203 ± 51	<1912	4

Table 3
$^{210}Pb_{ex}$ inventories (I), meteoric inputs, and calculated turnover times for $^{210}Pb_{ex}$ in the O horizon with respect to loss via advection. Meteoric inputs are determined by assuming that the whole profile is in equilibrium with the atmosphere: annual meteoric inputs = $\lambda_d I_{tot}$; Uncertainties on I_{tot} are calculated by propagating the measurement errors on the layers summed throughout the profile (Table 2). Mineral soil uncertainties are given in Table 2. Annual O horizon loss rates by advection are calculated as the amount of ^{210}Pb that decays in the mineral soil each year, and one sigma uncertainties on the turnover times are given in parentheses. ^{210}Pb measurements for Sites 1 and 2 were made during previous studies (†Kaste et al., 2003 and ‡Kaste et al., 2007).

Site	Total I (Bq m^{-2})	Meteoric inputs (Bq m^{-2} years^{-1})	Mineral soil I (Bq m^{-2})	O horizon advection loss (Bq m^{-2} years^{-1})	Steady-state fractional loss from O (% y^{-1})	Turnover time (y)
1.Camels Hump, VT†	16,300 (820)	506	795	25	0.16	627 (105)
2. Moosilauke, NH‡	9068 (323)	282	1400	44	0.57	174 (14)
3. Ducktrap, ME	7360(330)	229	2170	67	1.3	77 (9)
4. Mosvik, Norway	3540 (120)	110	203	6.3	0.19	530 (130)
5. Evje, Norway	3250 (162)	101	372	12	0.40	249 (43)
6. Birkenes, Norway	5750 (248)	179	1060	33	0.69	143 (18)
7. Amli, Norway	6950 (220)	216	2520	78	1.79	56 (7)

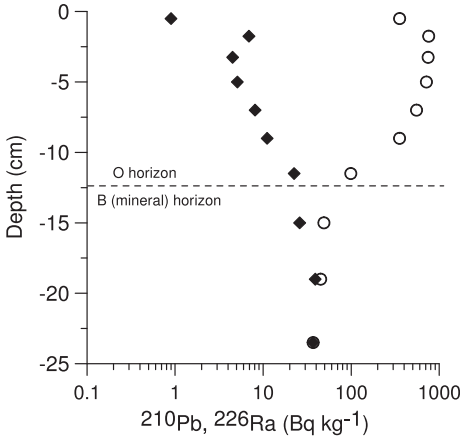

Fig. 1. ^{210}Pb (○) and ^{226}Ra (♦) with depth at Ducktrap. Analytical errors are smaller than the symbols.

presented in this paper at the Camels Hump. In that study, an enriched ^{207}Pb dose (92%) was applied to the soil surface in the coniferous forest zone at Camels Hump, VT in 1984. This area remained undisturbed until it was carefully sampled in 2001. The layer of soil at 4–8 cm depth had the majority the ^{207}Pb enrichment, and this layer was overlain by a section of buried flagging that was originally put on the surface in 1984. We treat this enriched ^{207}Pb layer to be the surface that was exposed to the dose in 1984 and subsequently buried by 17 years of litter inputs; the known soil layer age is used to evaluate the dating model applied in the current study. The quantitative recovery of the ^{207}Pb application confirms that soil erosion and sediment redistribution over the course of a few decades is minimal in this type of environment. Details on the radiogenic Pb isotopic measurements and recovery are given in Kaste et al. (2003).

3. RESULTS

3.1. Depth-profiles of atmospheric fallout in soils

3.1.1. Excess ^{210}Pb and NAE lead

The magnitude of $^{210}Pb/^{226}Ra$ disequilibrium in O horizon layers is large, indicating that virtually all of the ^{210}Pb in the O horizon is from the atmosphere. A high-resolution concentration-depth profile of ^{210}Pb and ^{226}Ra in a plot from the Ducktrap site is given to show the relative contribution of in-situ produced ^{210}Pb to total ^{210}Pb (Fig. 1) typical of profiles sampled in this study. ^{210}Pb in the O horizon was consistently one to two orders of magnitude higher than ^{226}Ra. In the upper mineral soil, the two nuclides begin to approach similar magnitudes; beneath ~20-cm depth all of the ^{210}Pb activity can be attributed to *in situ* production by ^{226}Ra (via ^{222}Rn). At depths below 25 cm $^{210}Pb/^{226}Ra$ generally varies slightly around a mean of 0.86–0.94 (data not shown), which indicates that 6–14% of the ^{222}Rn produced in soils diffuses into the atmosphere. In order to simplify our presentation and calculations, in this work, concentrations (Bq kg^{-1}) and amounts (Bq m^{-2}) of "excess" ^{210}Pb ($^{210}Pb_{ex}$) are calculated by subtracting ^{226}Ra activity from the total amount of ^{210}Pb activity. While this assumes that ^{222}Rn is in entirely in equilibrium

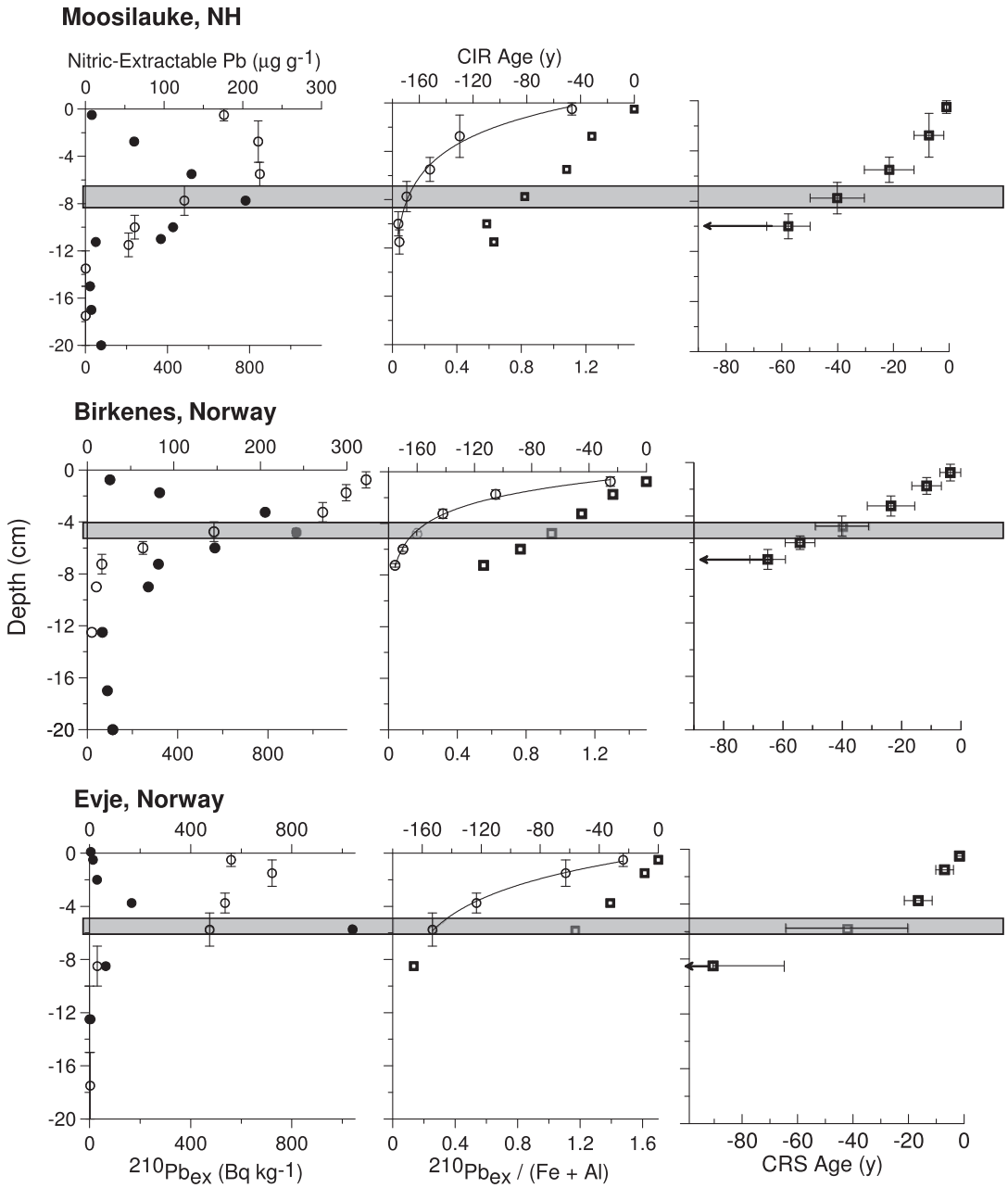

Fig. 2. Depth-profiles of $^{210}Pb_{ex}$ (○), and nitric-extractable Pb (●), left and dating model results (center and right panes). In the center pane, the $^{210}Pb_{ex}$ is normalized to (Al + Fe), and we apply a constant initial ratio model (CIR) to determine time, which assumes that the Al and Fe correct for litter decomposition and that radioactive decay governs the ratio. On the right side, a CRS dating model is applied to the raw $^{210}Pb_{ex}$ inventories measured in each horizon. The gray bar delineates the horizon in which the total extractable Pb was highest, which likely represents organic matter exposed during 1968–1978 at Moosilauke, and 1950–1965 at the Norway sites. The depth ranges given on the $^{210}Pb_{ex}$ points are laterally continuous.

with ^{226}Ra, the error introduced into our reported $^{210}Pb_{ex}$ values from this simplification will be very small because of the large difference between ^{210}Pb and ^{226}Ra. Other more detailed studies that account for radon diffusion have demonstrated that this assumption introduces a relatively small error (<15%) to inventory calculations even in non-organic soils (Nozaki et al., 1978). We propagate the errors associated with subtracting ^{226}Ra from ^{210}Pb using standard techniques (Appleby, 2001) discussed in detail in the Appendix.

Amounts of $^{210}Pb_{ex}$ in soil layers and horizons are given in Tables 2 and 3, respectively, and the data from Moosilauke, Birkenes, Evje, and Camels Hump are plotted in the left panels of Figs. 2 and 3. In general, 65–95% of the $^{210}Pb_{ex}$ inventory is in the O horizon. Excess ^{210}Pb within the O horizon has a distinctive distribution with depth,

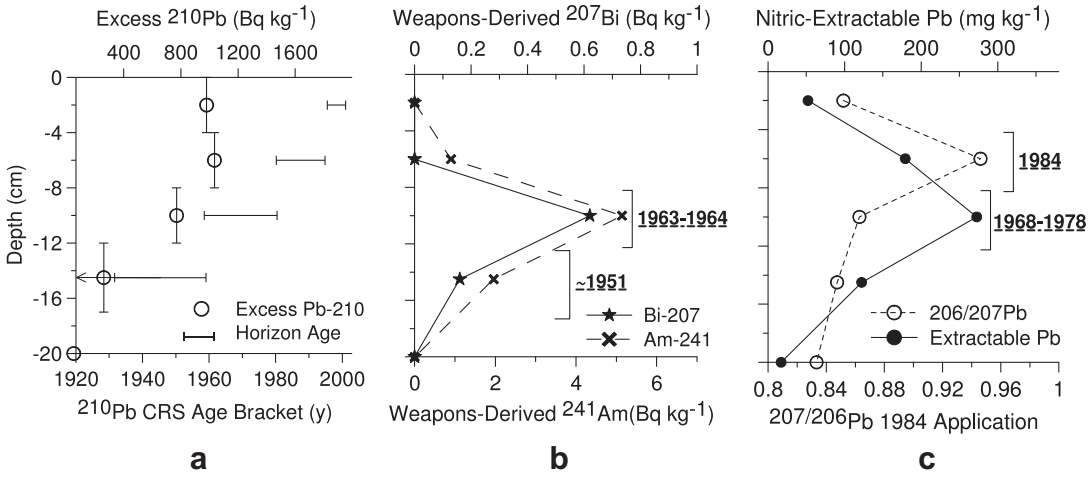

Fig. 3. Depth-profiles of $^{210}Pb_{ex}$ and $^{210}Pb_{ex}$-derived ages of 4 organic layers at Camels Hump (a). Depth-profiles of weapons-derived fallout nuclides ^{207}Bi and ^{241}Am (b), and nitric-extractable Pb and $^{207/206}Pb$ in the same layers at Camels Hump. The depth ranges given for the $^{210}Pb_{ex}$ points are laterally continuous across figures (a)–(c). This site received an enriched dose of ^{207}Pb at the surface in 1984, and the radiogenic $^{207/206}Pb$ and ^{210}Pb measurements have been reported previously (Kaste et al., 2003).

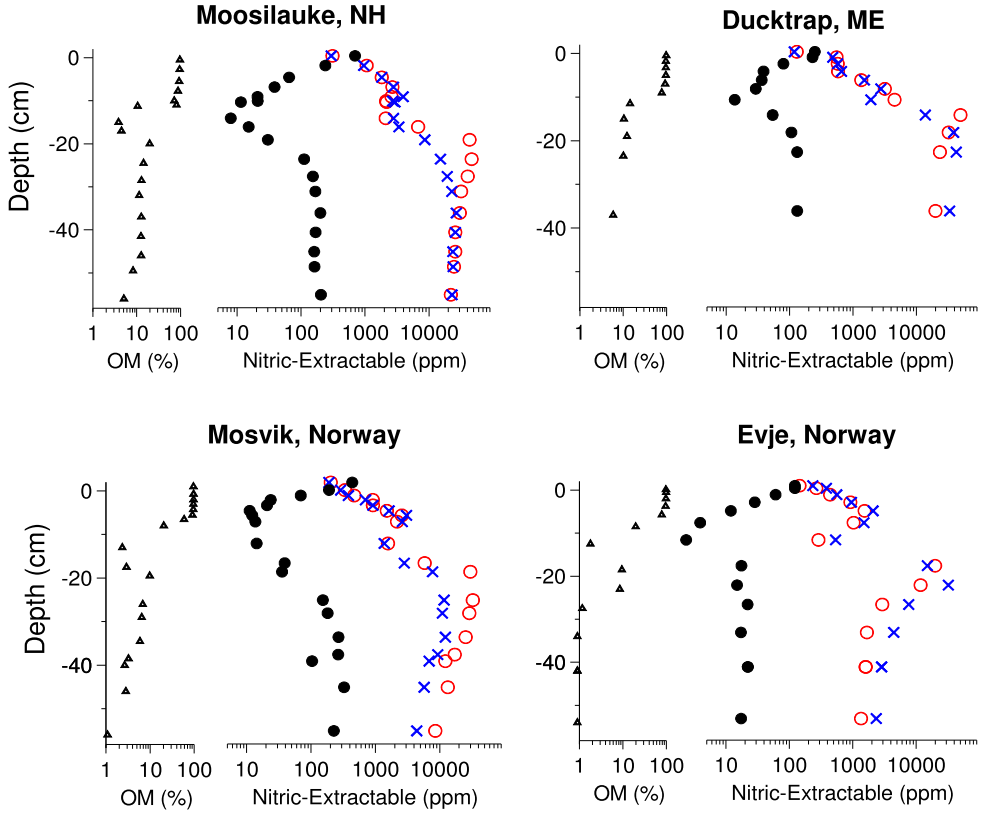

Fig. 4. Depth-profiles of organic matter (▲), and nitric-extractable Al (X), Fe (O), and Mn (●) at Moosilauke, Ducktrap, Mosvik, and Evje. All data used in these figures are given in the Electronic Annex.

where there is often a subsurface concentration maximum between 2 and 4 cm beneath the surface. In some cases $^{210}Pb_{ex}$ concentrations appear nearly homogenous in the upper 6-cm of the organic horizon, varying by ~20%.

It is important to note that this isotopic system of Pb is completely disconnected from the legacy of pollutant Pb in the environment and thus is useful even in areas that are largely free of atmospheric contamination. ^{210}Pb is

naturally present in the troposphere because of the decay of ^{222}Rn gas produced from the decay of ^{226}Ra. The amount of ^{210}Pb in air (Bq/m^3) at a particular location varies seasonally at mid to high latitudes by a factor of approximately 2, reaching a minimum in the spring/summer because of vertical mixing and washout (Sheets and Lawrence, 1999). While the seasonal variations of ^{210}Pb in air are significant, over timescales of years to decades, the quantity of ^{210}Pb in surface air and deposition rates (Bq m^{-2}) at a given location are relatively constant in the absence of major systematic changes in precipitation. The nearly constant flux of ^{210}Pb to the earth's surface, and its affinity to adsorb to particles has made it a valuable tool for quantifying the accumulation of organic and inorganic sediments in peatlands, lakes, and marine environments (Krishnaswami et al., 1971; Appleby, 2008).

The depth-distribution of NAE Pb is similar at all 7 of the sites we sampled in this study, and is controlled by the temporal distribution of pollutant Pb fallout (Table 2, and Figs. 2 and 3). In general, the upper 1–2 cm of the O horizon, which represents relatively recent litter has low NAE Pb contents, commonly 1–10 mg kg^{-1} (Fig. 2 left panel and Table 2). Beneath the fresh litter, there is a sharp concentration maxima where the NAE Pb content can reach >1000 mg kg^{-1} at 6 to 8-cm depth, and the Pb content decreases beneath this maxima. Detailed isotopic studies have demonstrated that nearly all of the lead in the organic horizons of the northeastern US and Norway is atmospherically-derived pollutant lead (Kaste et al., 2003; Steinnes et al., 2005), and deposition rates peaked in the northeastern United States between 1965 and 1975 and slightly earlier in Northern Europe (Shotyk et al., 2003; Cloy et al., 2008).

3.1.2. Cosmogenic ^{7}Be

Complete cosmogenic ^{7}Be ($T_{1/2}$ = 53 days) concentration-depth data are available for a subset of our profiles that we were able to analyze within 90 days of collection, before significant radioactive decay. Depth-profiles of ^{7}Be at Ducktrap and Birkenes are given in Appendix Fig. S1. Beryllium-7 is formed primarily in the stratosphere by cosmic-ray spallation of oxygen and nitrogen. Because of its source term and its short half-life, delivery to the earth's surface is strongest during convective storms and during the summer months which favor mixing between the upper and lower troposphere (Lal et al., 1958; Baskaran, 1995). We use this nuclide to put constraints on the maximum penetration depth of meteorically-delivered particle reactive elements in soils possible during a single storm. ^{7}Be is highly concentrated in the fresh forest litter (upper 1–2 cm of soil) at all sites, which is consistent with other studies (Wallbrink and Murray, 1996; Kaste et al., 2007). While we show data for two complete profiles, in all measured samples, greater than 85% of the ^{7}Be was in the upper 2-cm of soil, and ^{7}Be was never detectable (<1 Bq kg^{-1}) beneath 5-cm.

3.1.3. Weapons-derived fallout

Depth-profiles of weapons fallout isotopes ^{241}Am and ^{207}Bi are given for the Camels Hump Site in Fig. 3b and all of the ^{241}Am data are given in Table 2. The weapons-fallout concentration maxima traces organic matter that was exposed during early 1960s (Cambray et al., 1989). Similar to Pb, these atoms hydrolyze even in acidic soils and thus strongly adsorb to mineral or organic phases (Kim et al., 1997; Artinger et al., 2002). Because the input functions for gasoline-derived Pb and the weapons fallout can be treated essentially as single short-duration events, and the atoms are sequestered by forest vegetation (Russell et al., 1981), the distributions are similar in the soil profiles: a contaminated layer at depth is overlain by fresh "clean" litter, and underlain by even older material that pre-dates the era of peak atmospheric contamination. However, pollutant Pb and weapons-derived nuclides were introduced into the atmosphere over different time intervals, and thus provide independent constraints of forest litter "exposure" age.

3.2. Organic matter and geogenic elements in the soil profile

3.2.1. OM and NAE Al, Mn, and Fe

The distribution of OM in all profiles is given in Table 2. Nitric-acid extractable Al, Mn, and Fe concentrations in the Mooilauke, Ducktrap, Mosvik, and Evje profiles are plotted in Fig. 4 and tabulated in Appendix Table S1 and all metal pools are given in Table 4. The sharp boundary between the O horizon and the mineral soil can be seen in the organic matter content profiles (Table 2, Fig. 4, and Appendix Table S1). We consistently observed strong gradients of NAE Al, Fe, and Mn concentrations in the soil profiles. Nitric-acid extractable Al and Fe have very similar concentrations and depth distributions, despite significant differences in redox chemistry, mineral solubilities, and biological relevance. Clipped herbaceous vegetation and fresh litterfall (the uppermost 1-cm of the soil profile) have aluminum and iron concentrations ranging from 100 to 300 mg kg^{-1}. The transition from fresh litterfall to humified organic matter occurs within 10 cm of the surface, and the Al and Fe content of the most humified portion of the O horizon was commonly 1500–3000 mg kg^{-1}, which is an increase of 10–20-fold across this litter decompositional gradient. In the mineral soil immediately beneath the organic horizons, there is often a sharp drop in the Al and Fe concentrations in the eluviated (commonly referred to as an E or A2) horizon, attributed to the intense leaching that occurs immediately beneath the O horizon (Giesler et al., 2000). Underlying the ~2–5 cm E horizon, concentrations increase again in the upper mineral soil by a factor of ~10, reaching a maxima in the zone of illuviation (Bh(s) or other horizon) which was 20–30 cm beneath the surface at our sites. Beneath the zone of illuviation, levels of nitric-acid extractable Al and Fe decrease gradually towards background rock concentrations. At all of our sites, nitric-acid extractable Al and Fe varied by a factor of 100–300 in the upper 0.5 m of soil, showing systematic increases with depth in the O horizon, and increasing again beneath the eluviated horizon.

Nitric-extractable Mn concentrations have nearly the exact opposite trends of Al and Fe in the soil profile (Fig. 4 and Appendix Table S1). Manganese is present at higher

Table 4
Measured Al and Fe pools in the upper layer of the O horizon (left column) and in the entire O horizon (right column). Steady-state Al and Fe pools are calculated using the upper layer Al and Fe content, the age of this layer, and the turnover times given in Table 3.

Site	Deposition (atmospheric + litterfall) flux calculations				Calculated O horizon Al and Fe pools				Measured O horizon pools (total) ($g\ m^{-2} \pm 10\%$)	
	Measured upper O layer pool ($mg\ m^{-2} \pm 10\%$)		Years of record from ^{210}Pb dating	Calculated Deposition Flux ($mg\ m^{-2}\ years^{-1} \pm 15\%$)	Steady-state calculation from deposition ($g\ m^{-2} \pm 25\%$)		Estimated mineral-derived inputs ($g\ m^{-2} \pm 15\%$)			
	Al	Fe		Al	Fe	Al	Fe	Al	Fe	Al	Fe
Camels Hump	1884	3161	7	269	452	168	283	4	4	56	67
Moosilauke	178	186	3	59	62	8.5	8.9	3	4	26	21
Ducktrap	94	155	2	47	77	3.6	6.0	3	4	12	14
Mosvik	256	299	6	43	50	22.6	26.4	1	2	15	14
Evje	250	173	5	50	35	12.4	8.6	1	1	8.4	6.5
Birkenes	380	362	7	54	52	7.8	7.4	0.9	0.7	10.1	8.6
Amli	302	147	3	101	49	5.6	2.7	0.6	0.4	7.8	6.2

concentrations in clipped vegetation (~200–600 $mg\ kg^{-1}$) relative to Al and Fe, but Mn decreases rapidly with depth from the surface to the base of the O-horizon, by a factor of ~25 over only a few cm. Beneath the O horizon, NAE Mn then slowly rises in the mineral soil to levels approaching bedrock concentrations. Levels of NAE Mn in the upper 30-cm of mineral soil are two to three orders of magnitude lower than Al or Fe.

3.2.2. Thorium concentrations in O horizon profiles

The distribution of Th with depth at Ducktrap and Evje is illustrated in Appendix Fig. S2. In general, the Th content of O horizon layers is relatively low, ranging from undetectable to 3.5 $mg\ kg^{-1}$. Concentrations of Th in the mineral soil at a given site are relatively uniform with depth, typically in the 10–20 $mg\ kg^{-1}$ range. Within the O horizon, the Th content does not appear to increase systematically with depth. Rather, the Th content either remained unchanged with depth, or decreased with depth until the mineral soil boundary. We use Th concentrations as a proxy for mineral matter introduced by physical mixing between the mineral soil and O horizon.

4. DISCUSSION

4.1. Processes controlling the vertical distribution of $^{210}Pb_{ex}$ in O horizons

Atmospheric ^{210}Pb is deposited onto the soil surface with precipitation and as litter is dropped on the forest floor. One might expect $^{210}Pb_{ex}$ concentrations to steadily decrease with depth in the O horizon, since the horizon is layered with fresh litter on top, and older, and more humified organic material at depth. In soil profiles dominated by inorganic material, constant meteoric ^{210}Pb inputs and near-steady advection cause $^{210}Pb_{ex}$ concentrations in soils to decline monotonically with depth (Nozaki et al., 1978; Graustein and Turekian, 1986). Instead, in most of the O horizon profiles, we observe essentially the opposite trend, where $^{210}Pb_{ex}$ concentrations increase with depth in the upper ~5 cm (Figs. 1–3 and Table 2). In many cases, the highest concentration of $^{210}Pb_{ex}$ occurred in a very humified layer of organic matter (i.e., no recognizable needles, leaves, twigs, etc.), which we take to be forest litter that is on the order of one half-life old.

The presence of $^{210}Pb_{ex}$ sub-surface concentration maximums could perhaps be explained by episodic transport of ^{210}Pb in macropores during storm events (Bundt et al., 2000). If precipitation events of different size and intensity deliver atmospheric Pb to different depths on short timescales, then the vertical distributions we observe could be produced. We use cosmogenic ^{7}Be to evaluate how event-driven macropore flow could potentially control the initial distribution of atmospherically deposited Pb atoms with depth in the O horizon. Both Be and Pb have very high solid:solution partitioning behavior of 10^3–10^5 ($kg\ l^{-1}$) even in slightly acidic environments (Hawley et al., 1986; You et al., 1989; Sauve et al., 2003), and are strongly hydrolyzing. This similar affinity for inorganic and organic surfaces has led a number of researchers to use the ratio of $^{7}Be/^{210}Pb$

measured on particles as a "clock" for calculating particle transit times on short (<years) timescales (Bonniwell et al., 1999). Our ^{7}Be data show how rapidly metals can be fixed to organic matter upon deposition (Appendix Fig. S1), very similar to what others have found in different environments (Wallbrink and Murray, 1996). We maintain that the depth-distribution of ^{7}Be represents a maximum initial depth-distribution of atmospherically deposited Pb in soils, because ^{7}Be fluxes to earth's surface are largest during intense precipitation events. Unlike ^{210}Pb, there is more ^{7}Be in the stratosphere than troposphere, thus ^{7}Be tends to be more concentrated in thunderstorms and has a smaller proportion of dry deposition (Lal et al., 1958; Brown et al., 1989; Baskaran, 1995; Kaste et al., 2002).

Given the limited penetration of ^{7}Be in the O horizon, the strong partitioning of Pb to organic matter (Kerndorff and Schnitzer, 1980; Sauve et al., 2000), the importance of dry deposition for atmospheric Pb (Miller and Friedland, 1994) and the long residence time of atmospheric Pb reported for O horizons (Wang and Benoit, 1997; Kaste et al., 2003, 2006a; Klaminder et al., 2006), it is unlikely that Pb is transported to significant depths in the soil following deposition. It is more likely that Pb is bound strongly to the initial surfaces that it comes into contact with, that is, live leaves and surface litter (Russell et al., 1981). As leaves containing Pb are buried by subsequent years of litterfall, Pb is quantitatively retained by the material. In a 57 month decomposition experiment of Red Spruce litter, Rustad (1994) demonstrated that Al and Fe were enriched in the organic matter over time as carbon and other labile elements were lost. They suggested that retention was controlled by abiotic adsorption onto litter exchange sites. Lead also has a very strong affinity for organic matter functional groups (Kerndorff and Schnitzer, 1980; Manceau et al., 1996; Sauve et al., 2000), and could reasonably be expected to behave in a similar manner. Recent experimental work has demonstrated that initially, atmospheric Pb may be bound to organic matter functional groups, but after a few years of decomposition, Pb speciation may shift towards bonding with secondary Fe oxide minerals coating the litter (Schroth et al., 2008). A large number of previous studies have concluded that Pb is effectively retained on organic matter, and its subsequent transport in the profile is limited by the transport of organic matter itself (Dorr and Munnich, 1989; Miller and Friedland, 1994; Wang and Benoit, 1997; Kaste et al., 2003, 2006a).

Because organic matter can lose 20–50% of its carbon in the first year of oxidation (Schlesinger, 1977), and the half-life of ^{210}Pb is 22 years, organic matter decomposition causes a relative enrichment over the first few years of burial (Fig. 5). The depth-concentration profiles of ^{210}Pb$_{ex}$ in decomposing horizons of organic matter are best described with a model of decomposition-radioactive decay, rather than advection–diffusion-radioactive decay, where $f(t)$ represents the fraction of organic matter remaining relative to freshly deposited surface litter (Fig. 5; Appleby and Oldfield, 1992; Kaste et al., 2007):

$$C(t) = \frac{C_o \exp[-\lambda t]}{f(t)} \quad (1)$$

Under the combined processes of OM decomposition and radioactive decay, depth-concentration profiles of ^{210}Pb$_{ex}$ are related to the rate of OM accumulation, which determines the overall thickness of a deposit, and decomposition, which determines the extent of enrichment and the depth of subsurface concentration maxima (Fig. 5). In such a model, the ^{210}Pb$_{ex}$ concentration in a layer (C, in Bq kg^{-1}) is a function of its original concentration (C_o, in Bq kg^{-1}), age, extent of organic matter decomposition (causes $f < 1$), and possibly dilution from below-ground mass inputs that are low in ^{210}Pb$_{ex}$ from processes such as physical mixing and root growth (causes $f > 1$). Using experimental data from Rustad (1994), where organic matter decomposition is described as a two-stage process, with a fast initial decay rate (0.17 years^{-1}) followed by slow decay (0.02 years^{-1}) the general form of the ^{210}Pb$_{ex}$ distribution with depth that we measured is approached (Fig. 5). This helps us develop a mechanistic model that describes the behavior of atmospherically-deposited Pb in O horizon layers, but in practice, it would be difficult to describe $f(t)$ accurately enough to use Eq. (1) to calculate reliable soil layer ages.

4.2. Applying a steady-state ^{210}Pb$_{ex}$ box model to quantify the timescale of mobile organo-metallic colloid production in the O horizon

Our data considered within the context of previous work are consistent with the mechanistic model that after deposition on the O horizon surface, Pb atoms are retained by the upper litter layer and concentrations rise as this litter is buried and decomposes. However, the presence of small but significant ^{210}Pb$_{ex}$ inventories in the mineral soil layers immediately beneath the O horizon (Figs. 1–3, and Tables 2 and 3) is strong evidence that there is a transfer of ^{210}Pb$_{ex}$ from decomposing organic matter to underlying mineral layers. Field and laboratory-based studies have demonstrated that the dissolved transport of ionic Pb^{2+} is negligible compared with particulate ^{210}Pb transport even in slightly acidic O horizons (Wang et al., 1995; Wang and Benoit, 1997; Kaste et al., 2005); Pb transport from the O horizon to the mineral soil is most likely in the form of an adsorbed complex on organo-metallic colloids (Bargar et al., 1997a, 1997b; Kaste et al., 2006a). Previous work has shown that the movement of atmospheric Pb in the soil profile may be controlled at least in part by organic matter decomposition rates (Dorr and Munnich, 1989; Miller and Friedland, 1994; Kaste et al., 2006a). If the transfer of ^{210}Pb from the O horizon to the underlying mineral soil is limited by the production of mobile organo-metallic colloids from canopy-derived litter, then we can quantify this process using a first-order removal constant (λ_l) that represents the advection of organo-metallic colloids with ^{210}Pb$_{ex}$. The steady-state ^{210}Pb$_{ex}$ budget of the O horizon is:

$$\frac{dI^{210}\mathrm{Pb}_O}{dt} = F - (I^{210}\mathrm{Pb}_O\lambda_d + I^{210}\mathrm{Pb}_O\lambda_l) = 0 \quad (2)$$

where I^{210}Pb$_O$ is the inventory of ^{210}Pb$_{ex}$ in the O horizon (in Bq m^{-2}), F is the steady-state meteoric flux of ^{210}Pb to the soil (in Bq m^{-2} years^{-1}), λ_d is the radioactive decay loss constant for ^{210}Pb (0.0311 years^{-1}), and λ_l is the rate loss

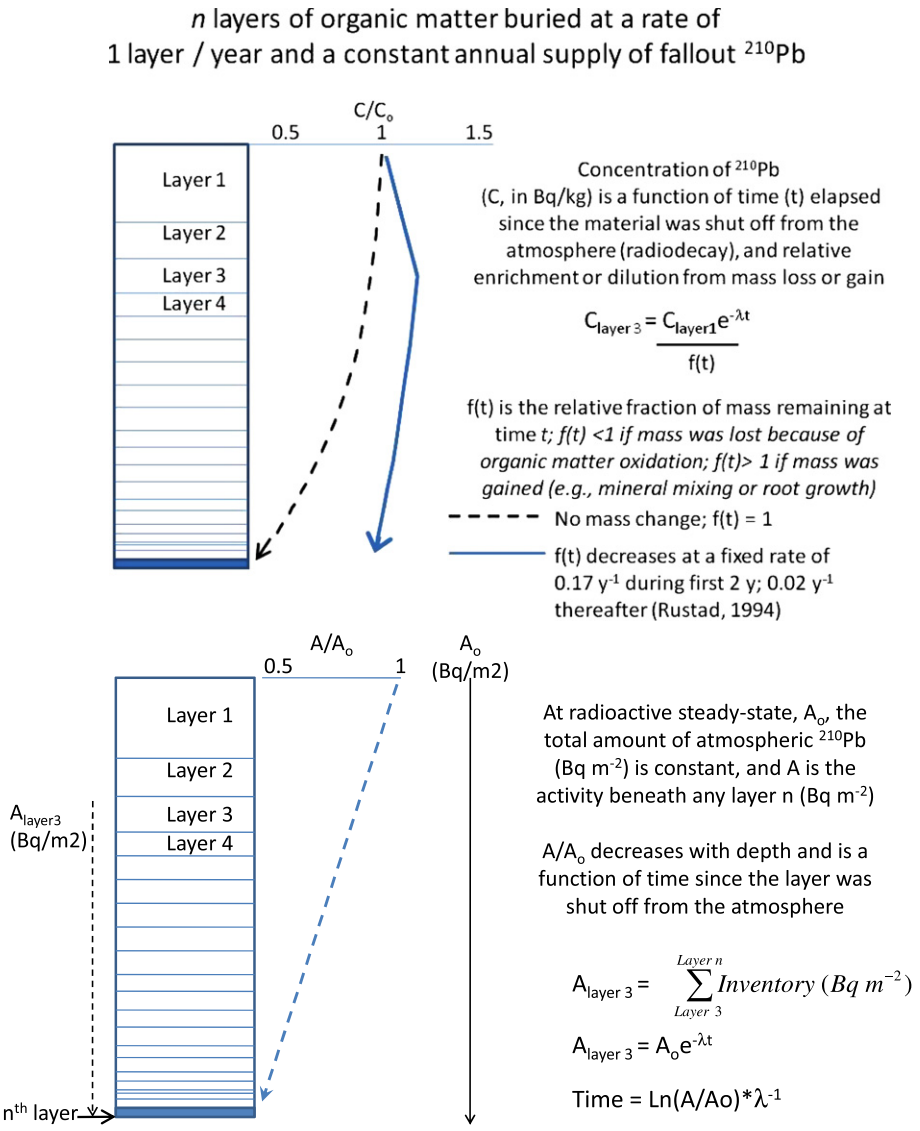

Fig. 5. Two different steady-state models that describe the distribution of $^{210}Pb_{ex}$ with depth in soils. Concentration-based models (upper) require an organic matter decomposition function in order to capture the form of the concentration-depth profiles we measure here (Figs. 1–3). Inventory-based models such as the CRS (lower) are not effected by organic matter decomposition, but rely on the assumption that surfaces no longer receive atmospheric ^{210}Pb inputs after burial.

constant for ^{210}Pb advected out of the O horizon. This model assumes that the standing crop of $^{210}Pb_{ex}$ in the mineral soil is in steady-state with advected particles coming in from the base of the O horizon, and that the whole profile is in steady-state with atmospheric inputs. These assumptions are reasonable because our sites have been undisturbed (forested) for at least 60 years, and the total inventories we report here are generally compatible with steady-state fluxes reported by others who measured soils or deposition rates at similar elevations and longitudes (Graustein and Turekian, 1986; Preiss et al., 1996). While the total variability in $^{210}Pb_{ex}$ inventories we report here is wide, varying by a factor of 3 across our sites in New England, atmospheric ^{210}Pb fluxes are a function of air mass source, rainfall rates, occult deposition, and other factors that can vary dramatically in complex terrain. Graustein and Turekian (1986) reported $^{210}Pb_{ex}$ inventories in soils from Whiteface, Camels Hump, and Moosilauke to range from 4900 to 12,000 Bq m^{-2}, which are similar values to our total surface inventories given in Table 3. While the spatial and seasonal variability of ^{210}Pb deposition is significant and complex, our only assumption is that ^{210}Pb deposition at a single soil plot varies around a mean and is not systematically changing over time. Long-term monitoring (>10 years of data) of ^{210}Pb concentrations in air have shown strong seasonal variability but no measurable change on decadal timescales (Sheets and Lawrence, 1999), which supports our assumption stated above.

In this steady-state box model, the loss rate (λ_l) is determined by calculating the amount of $^{210}Pb_{ex}$ required to

advect out of the O horizon to replenish radioactive decay in the B horizon (Table 3), and annual meteoric inputs are calculated as the flux of ^{210}Pb required to replenish the annual decay of $^{210}Pb_{ex}$ in the entire soil profile. Annual steady-state $^{210}Pb_{ex}$ loss rates (via advection) from the O horizon, calculated by dividing the advection flux (Bq m^{-2} years^{-1}) by the O horizon $^{210}Pb_{ex}$ pool (Bq m^{-2}, in Table 3 this is the difference between *total I* and *mineral soil I*), range from 0.16% to 1.79%. We calculate turnover times using these data, which are the inverse of the loss rate for each site, to range from approximately 60–630 years (Table 3). Organic horizon turnover times calculated using the $^{210}Pb_{ex}$ box model described here put a timescale on a very critical process regulating the production of mobile organo-metallic colloids from fresh litter, and this timescale can be used to model the fate of other strongly hydrolyzing metals that are delivered to the O horizon surface on fresh litter. It is interesting to note that sites with the smallest loss rates and thus the longest turnover times are Sites 1–2 in New England that were at relatively high elevation (>900 m) and our northern most site in Norway (Mosvik), which are in environments where decomposition rates are expected to be lowest (Schlesinger, 1977). These data appear to support a connection between organic matter turnover and contaminant release from soil reservoirs.

4.3. ^{210}Pb dating in O horizon layers

While fallout radionuclides have been used extensively to date lake sediments, peat deposits, and quantify marine sedimentation and mixing rates, the application of these tracers to quantify soil processes has been very limited. Given the assumptions that we justify above on the quantitative retention of atmospheric Pb in decomposing litter, and the lack of episodic advection and mixing we infer using other tracers, the upper part of the O horizon in soils sampled here may be suitable for ^{210}Pb dating using a steady-state deposition model. A number of very recent works have shown that the layers of litter in "mor-type" soil horizons (those in which the organic horizon is clearly distinguishable from the underlying mineral horizon) do in fact record a stratigraphy of atmospheric deposition and soil organic matter inputs (Kaste et al., 2007; Klaminder et al., 2008, 2009; Klaminder and Yoo, 2008).

As discussed earlier, the concentration maxima of $^{210}Pb_{ex}$ just beneath the surface in these soils is likely controlled by the more rapid decay of organic matter compared to the radioactive decay of $^{210}Pb_{ex}$ during the first few years of decomposition. Iron and Al are also immobile in decomposing organic matter (e.g., Rustad, 1994) and sorption experiments suggest that the binding affinities of Al, Fe, and Pb are similar for humic substances (Kerndorff and Schnitzer, 1980). As such, their concentration profiles in the soil should be similarly affected by organic matter decomposition. When $^{210}Pb_{ex}$ is normalized to nitric-extractable Fe + Al, a more classic logarithmic depth-decay form is obtained (Fig. 2, middle). When we apply a simple constant initial ratio (CIR) age model, which assumes that incoming litter has a constant ^{210}Pb/(Fe + Al) value, and all three elements are enriched identically with organic matter decomposition, then we can get a distribution of age with depth (Fig. 2, middle) which we test below with independent tracers.

Another approach to ^{210}Pb dating is a constant rate of supply age model (Krishnaswami and Lal, 1978; Oldfield et al., 1978; Robbins, 1978) which is not affected by relative enrichments from organic matter decomposition or dilution from material introduced from below (CRS, Fig. 5). The CRS model calculates surface ages using $^{210}Pb_{ex}$ inventories (A, units of Bq m^{-2}) measured in each layer. It requires radioactive equilibrium between the soil and the atmosphere, and near-constant deposition of ^{210}Pb to the surface each year (Bq m^{-2} years^{-1}), where A is the inventory beneath a buried surface, $A(0)$ is the steady-state inventory of the entire profile, and t is the age that the now buried surface that was at one time exposed.

$$A = A(0)e^{-\lambda t} \tag{3}$$

This model assumes that the whole soil profile is in steady-state with the inputs from the atmosphere and we justify this assumption in our box-model description above. We present several lines of independent evidence to check the ages of organic soil layers determined by the two different ^{210}Pb dating models (CIR and CRS) in the well-drained environments that we sampled here. One such independent constraint is based on the period of atmospheric Pb deposition. While we do not report on radiogenic Pb isotopes here, which would provide a more robust quantification of the sources of Pb in the soil samples, we can use the depth-profile of NAE Pb to broadly define the distribution of pollutant Pb in the upper part of the profile. This is reasonable because previous detailed radiogenic Pb studies have shown that virtually all of the Pb in the O horizon layers at our sites is from air pollution, and even in the upper mineral soil, pollutant Pb can comprise the majority of the Pb extracted by an acid extraction that does not completely dissolve the primary minerals in the sample (Kaste et al., 2003; Steinnes et al., 2005).

The shaded bar in Fig. 2 marks the horizon in which peak levels of NAE Pb were extracted. In all cases, the CIR model returned much older dates for the NAE Pb rich horizons than would be expected. For example, the mean CIR date for the NAE Pb rich layers was 1920 at Moosilauke, about 50 years prior to the known period of maximum Pb deposition. Similarly, the CIR-calculated dates of Pb-enriched soil horizons in the Birkenes (1938) and Evje (1947) site also overestimated age by several decades (Fig. 2, middle). The failure of the CIR age model to accurately predict soil ages reflects an error in one or more of underlying assumptions of the model. In this case, it appears that there may be an additional source of Al and Fe that influences the calculated soil age. Dividing the $^{210}Pb_{ex}$ concentrations by (Al + Fe) normalizes for relative concentration enrichments, assuming that Pb, Al, and Fe are all are derived from similar sources and behave similarly during decomposition. However, if Al and Fe are added from below-ground sources then it would dilute the ^{210}Pb/(Al + Fe) values, making deeper horizons appear older than they are. We do not think that this phenomena can be explained by a higher mobility of Pb compared with

Al and Fe, because all three metals are projected to form equally strong complexes with organic matter functional groups (Kerndorff and Schnitzer, 1980) and, if anything, Al solubility (with respect to Al hydroxide) would be higher than Pb solubility in the slightly acidic soils that we study here (pH = 4–5). Rather, we suggest that below-ground inputs of Fe and Al to the organic horizons represent significant contributions to their respective inventories, and such inputs could be important to the development of Spodosols. We evaluate the possible sources of Al and Fe to O horizon layers in Sections 4.4 and 4.5.

The CRS model returned more reasonable ages for the NAE Pb rich organic layers (Table 2). Specifically, at Moosilauke, Birkenes, Evje (Fig. 2), and Camels Hump (Fig. 3), ages ranges were 1963–1978, 1965–1976, 1934–1976, and 1958–1976 for the layer of soil containing the highest amounts of NAE Pb. At Amli, much of the NAE Pb, on a mass basis, appears to be in the mineral soil (A horizon and lower) and the age of the lower most O horizon layer was 1971. This site was in a Scots Pine Stand, and perhaps more rapid decomposition has resulted in the transfer of organic matter containing pollutant Pb out of the O horizon and into the minerals soil. It is important to note that we only use the CRS model to determine the ages of layered O horizons: all of the $^{210}Pb_{ex}$ in mineral horizons (A and B horizons) was combined into the lowest layer that has no lower boundary for age (indicated by arrows in Figs. 2 and 3).

At Camels Hump we make use of an enriched ^{207}Pb dose that was applied to the soil surface (upper layer of forest litter) in 1984 and recovered in 2001 (Kaste et al., 2003). This manipulation study also helps confirm the utility of CRS based soil ages. Fig. 3c shows that most of the ^{207}Pb was recovered at 4–8 cm; we interpret this layer to represent surface litter from 1984. The ^{210}Pb CRS model date for this layer is 1979–1995 (Fig. 3a and Table 2). The application was small enough that it did not affect the total Pb content of the soil, which is governed by the temporal distribution of atmospheric Pb pollution in the region. Nitric-extractable Pb peaked in a horizon that had a $^{210}Pb_{ex}$-derived age of 1952–1979, consistent with the peak of atmospheric contamination around 1970 (Figs. 2 and 3). In that study, a detailed radiogenic Pb isotopes confirmed that essentially all of the Pb in the O horizon was from leaded gasoline, and most of this Pb was still in the O horizon (Kaste et al., 2003).

We use depth-profiles of weapons-derived fallout radionuclides as another independent check on the reliability of the CRS ^{210}Pb chronology (Table 2). The weapons-fallout concentration maximum traces organic matter that was exposed during the early 1960s, which is the time period of the highest atmospheric contamination from weapons tests (Cambray et al., 1989). Fig. 3b shows activity-depth profiles of weapons-derived ^{241}Am and ^{207}Bi at the Camels Hump Site. The layer with the highest ^{241}Am and ^{207}Bi inventories had a CRS ^{210}Pb derived age of 1952–1979, and a portion of the total ^{241}Am and ^{207}Bi inventories were recovered in the lowest O-horizon sample which had a ^{210}Pb age of $\leqslant$1952 (Fig. 3). The Camels Hump soil profile preserved sharp concentration maximums of 4 temporally distinct tracers that are all well-documented to strongly bind to organic matter (Appleby et al., 1991; Kim et al., 1997; Sauve et al., 2000; Artinger et al., 2002), suggesting that Coniferous O horizons can record a stratigraphy of litter inputs and atmospheric fallout elements that bind strongly to organic matter in the upper layers. It is interesting to note again, that at Amli, which had the "youngest" O horizon layers (Table 2) had most of the NAE Pb and the ^{241}Am inventory in the upper mineral soil (A + Bs), which, shows how rapid O horizon turnover can result in the transfer of elements to the mineral soil. In all, NAE Pb, and weapons-derived ^{241}Am at the other sites provide multiple independent means of determining the age of soil organic soil horizons, and are consistent with the CRS model (Table 2).

Organic horizon layer ages determined by the CRS ^{210}Pb model are constrained on the high and low ends by the average time elapsed since the surface above and below the layer stopped receiving atmospheric inputs of ^{210}Pb; the CRS ages may thus be interpreted as average burial ages. Because the residence time of some organic matter in the lower O horizon layers can be considerably longer than the half-life of ^{210}Pb, and the presence of old organic matter in the profile does not impact the CRS date, O horizon layers can contain some organic matter that is older than the burial age. Litter decomposes in two stages, with relatively rapid decomposition during the first few years followed by decades to centuries of a much slower decay rate (Rustad, 1994; Currie and Aber, 1997), so we expect this effect to be largest in the deepest, more humified O horizon layers. Generally, O horizon humus layers have CRS ages between 40 and 90 years, but bulk O horizon ^{210}Pb turnover times range from 60 to 630 years (Table 3). The very long turnover times of O horizon ^{210}Pb compared with average humus layer CRS ages is caused by the fact that only the oldest organic matter is advected from the O horizon to the mineral soil beneath.

Not surprisingly, the lowermost layers within an O horizon profile have wider age brackets, on the order of 15–50 years because of higher density of humus compared with fresh litter. The oldest O horizon humus layers differ in age by approximately a factor of two to three from site to site. For example, the humus layer at the base of the O horizon at the Amli, Norway site had a CRS age of 1971–1983, while humus at the base of the O horizon sampled from Mosvik, Norway had a CRS age of 1912–1940. This difference is consistent with a faster decomposition in Pine forests compared with Spruce forests (Berg, 2000). The CRS ages of the lowest humus layers in the O horizon are the ones that are most susceptible to being affected by advection. We have developed a model where ^{210}Pb is advected from the base of the O horizon to the mineral soil in an organic (complexed) form. For the CRS ages to be most valid, the lower O horizon layer must be in steady-state with respect to ^{210}Pb and organic matter, and ^{210}Pb must trace the organic matter mass transfer. However, if ^{210}Pb is moving in a process decoupled from the organic matter transfer (as Pb^{2+} for example), then the calculated age of this layer would be younger than the burial time. If

this is suspected, then one could use the base of the O horizon as the lowest dated layer, and include the inventory beneath it to calculate the widest possible date bracket.

4.4. Using O horizon dating to describe the sources and fate of aluminum, iron, and manganese in decomposing organic matter

The transport and fate of Al, Fe, and Mn in watersheds have significant ramifications for the health of terrestrial and aquatic ecosystems (Sherman et al., 2006), but the role that the biosphere has on regulating the dynamics of these elements remains poorly constrained (Li et al., 2008). Iron and Mn are elements that are critical in trace amounts for photosynthesis and the production of a number of amino acids (Abadia, 1991). In contrast, high levels of dissolved Al can be toxic to forests (Shortle and Smith, 1988), aquatic ecosystems (Baker and Schofield, 1982), and can inhibit microbial processes critical to the biogeochemical recycling processes (Brynhildsen and Rosswall, 1997). Oxides of Al, Fe, and Mn have significant reactive surface area capacity that can sequester nutrients and contaminants in terrestrial ecosystems, and have been documented to play critical roles in the cycling of P (Giesler et al., 2002; Peretyazhko and Sposito, 2005), Pb and other toxic elements (Bargar et al., 1997a, 1997b), and carbon (Kleber et al., 2005). Recent work has demonstrated that soil humus has very high levels of secondary aluminum and iron, but the precise mechanisms by which humus accumulates metals is not well understood (Giesler et al., 2000). Because of the critical role that these metals can play in the cycling of nutrients and contaminants in soils, and our incomplete understanding of the biogeochemical cycling of metals, new techniques are being developed to partition the different processes that control the fate of these metals at the earth's surface (Wiederhold et al., 2007).

Aluminum, Fe and Mn concentrations have consistent and distinct trends with depth in the soil profiles (Fig. 4 and Appendix Table S1). Metal inputs to the top of the O horizon result from litterfall and wet and dry deposition. While the exact partitioning of these processes as sources of metals to the top of the O horizon are not entirely constrained, detailed budget studies in coniferous watersheds have shown that biocycling and litterfall make up a larger flux of these metals to the O horizon compared to bulk atmospheric deposition (Rustad and Cronan, 1989). In the O horizon, concentration gradients in layers are controlled by some combination of (a) uptake by vegetation, (b) relative enrichment with loss of CO_2 (Rustad, 1994), (c) physical soil mixing, (d) below-ground biological circulation (Vogt et al., 1987; Fimmen et al., 2008), and (e) leaching. In the upper mineral soil beneath the E horizon, Al and Fe concentrations reach a maximum because of illuviation processes (Lundstrom et al., 2000; Donisa et al., 2005), while Mn appears to be strongly depleted with depth. By combining the chemical profiles (Fig. 4) and the results of the CRS ^{210}Pb dating model (Table 2), we can convert depth in the O horizon to organic matter age, and gain valuable insight as to the timescale of processes that regulate Al, Fe, and Mn in decomposing litter (Figs. 6 and 7).

According to the CRS ^{210}Pb-derived ages, the Mn content of decomposing organic matter declines nearly exponentially with time, decreasing by ~50% within the first decade of decomposition, and leveling off at 4–6% of its initial value after 40 years (Figs. 6 and 7). The normalized Mn data showing relative concentration changes over time (Fig. 7) are remarkably consistent from site to site. One possible mechanism for the rapid loss of Mn from decomposing litter is tight recirculation by the forest ecosystem. This tight recycling would help explain the lack of an accumulation layer of Mn in the upper mineral soil, and the low concentrations of Mn typically found in surface waters of boreal forests (Bjorkvald et al., 2008). Mn has a much lower affinity for organic matter compared with Al or Fe (Kerndorff and Schnitzer, 1980), so dissolved losses of Mn from decomposing organic matter, as either a simple ion or a soluble complexed form may also be responsible for its depletion with depth in the O horizon. We note that there is no obvious zone of Mn accumulation in the mineral soil as we see for Al and Fe, so it does not appear to be significantly translocated.

In contrast to Mn, Al and Fe increase approximately linearly (Figs. 6 and 7) with organic matter age. In all cases, the Al and Fe content of litter increases by a factor ~5 in the first decade of decomposition. This enrichment would be expected if Al and Fe are quantitatively retained as C, O, and N are lost during the first stage of oxidation. The decomposition of coniferous forest litter is often modeled as a two-stage process, with an initial rapid stage where ~80% of the mass is lost (Berg, 2000). The initial stage is followed by a much slower stage of decomposition where mass loss rates might be ~0.01 years^{-1} (Currie and Aber, 1997). Our profiles of fallout lead and radionuclides are consistent with the premise that decomposition drives a relative enrichment of certain metals in the profile (Figs. 1–4). However, relative concentration increases resulting from mass loss can only explain about half of the Al and Fe accumulation observed in the O horizon, because decomposition-based mass loss is usually limited to 80–85% on timescales of decades, which would limit the concentration of Al and Fe in humus to be approximately 5× the concentration of fresh litter, while total Al and Fe enrichments can exceed 10–20 times initial concentrations (Figs. 6 and 7).

While there is considerable variability in the rates of Al and Fe enrichment across the sites (Fig. 7), generally after the initial decade of decomposition, organic matter continues to accumulate Al and Fe. However, the high concentrations of Al and Fe in base of the O horizon (OM ages >20 years) are inconsistent with solely a decomposition-based enrichment mechanism. While there is indeed measurable mineral matter in the O horizon layers (typically 4–15% mass remains after ashing in the upper O horizon layers (Table 2), measurements of NAE Al and Fe in the soil profile suggest that physical soil mixing is not a likely process for increasing the metal concentration of O horizon humus, because the highly leached E horizon, which is the material that would be most likely mixed into the O horizon, is actually lower in NAE Al and Fe than the O horizon humus (Fig. 4 and Appendix Table S1). Furthermore, profiles of fallout radionuclides and Th are evidence against

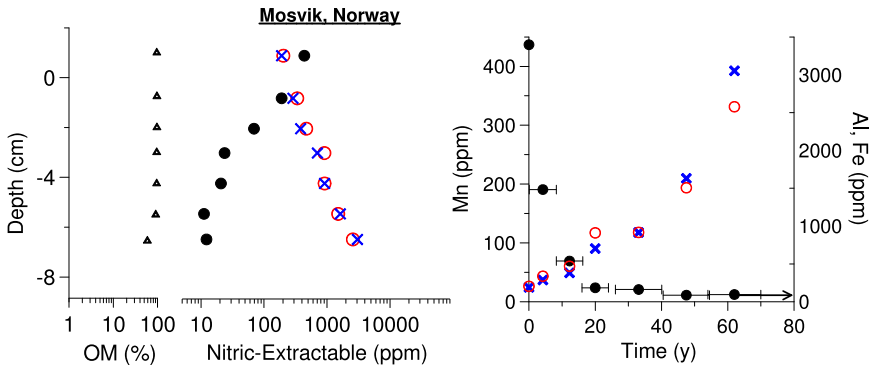

Fig. 6. Al (X), Fe (O), and Mn (●) with depth (left) and age (right) in the O horizon at Mosvik, Norway. The $T = 0$ sample was determined by measuring live vegetation. Age brackets given on the Mn data (right) are applicable to the Al and Fe data.

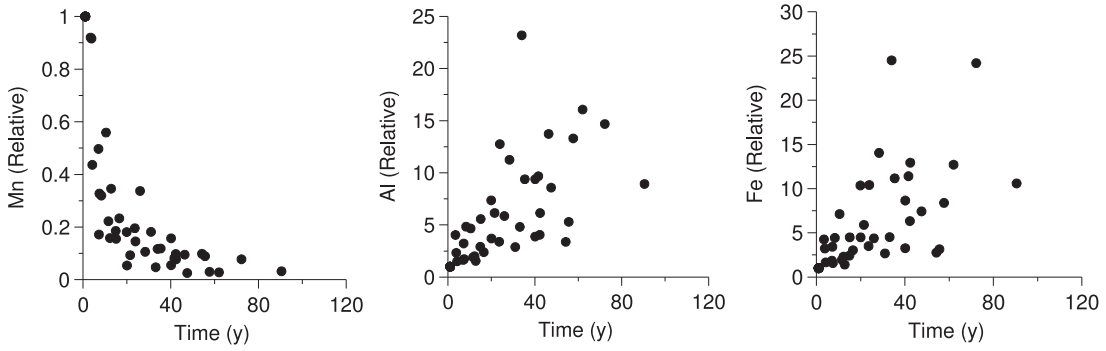

Fig. 7. Evolution of Mn, Al, and Fe in the O horizon layers with median age for each layer (ages and uncertainties given in Table 2). O horizons chemistry from all sites are plotted with elemental compositions normalized to the freshest litter collected.

significant physical mixing of mineral matter into the lower parts of the O horizon on short-timescales. Much of the mineral matter that is in the O horizon may be from episodic events, such as tree throw, which is not a mechanism capable of producing the systematic concentration gradients of Al and Fe observed here.

4.5. Modeling steady-state O horizon Al and Fe pools from bulk deposition

Our data can be used to assess the relative sources of Al and Fe to O horizons. We use the dated upper-most O horizon layer collected at each site to calculate a combined litterfall and atmospheric deposition flux for Al and Fe. This layer, which was typically the upper one to two cm of fresh and partially decayed leaf litter is almost entirely organic matter, and should have minimal elemental contributions from below-ground sources such as physical soil mixing or even root growth (Table 2). The number of years of deposition that this surface layer represents is constrained using ^{210}Pb CRS chronology (Table 2), and depositional fluxes are calculated by dividing the Al and Fe pools in this upper layer by the layer age. By calculating fluxes in this manner, it incorporates wet deposition, dry deposition (including dust), and Al and Fe deposited on the surface by litterfall, assuming that all of the Al and Fe remained in the litter as it decomposes. One-sigma uncertainties in the pools are dominated by the bulk density uncertainty (10%), which, when propagated with the CRS age uncertainty (Table 2) result in an average 15% uncertainty in the depositional flux. With only a few exceptions, our calculated depositional fluxes of Al and Fe range between 40 and 100 mg m^{-2} years^{-1} (Table 4), which agree remarkably well with wet and dry fluxes measured directly by others in similar environments (Rustad and Cronan, 1989; Duce and Tindale, 1991; Berg et al., 1994; Li et al., 2008). Most notably, Rustad and Cronan (1989) monitored monthly wet and dry deposition, litterfall, and canopy throughfall for two years at a nearby and similar site to Ducktrap, and determined total Al and Fe deposition fluxes to be 50 mg m^{-2} years^{-1} each, which essentially matches our calculated values (Table 4).

Steady-state Al and Fe pools that accumulate in the O horizon from deposition (litterfall + atmospheric) are determined using the steady annual inputs calculated with the Al and Fe measurements in the dated top layer of the O horizon and the ^{210}Pb-derived loss rates (λ_l, Tables 3 and 4). Uncertainties in the steady-state pool projections as calculated by propagating the uncertainty in the depositional flux with the uncertainties in the turnover times (Table 3) average 25%. Another obvious source of Al and Fe to the O horizon apart from deposition is the physical mixing of mineral matter into the horizon from beneath. We estimate Al and Fe contributions to the O horizon from

minerals mixed in from belowground using the mineral content of the O horizon (Table 2) and the Al and Fe content of the upper mineral soil. We argue that this calculated mineral-derived Al and Fe pool represents an upper limit, because it uses the concentration in the upper mineral soil (the layer most likely to be mixed into the O) and assumes that the metals are never lost, essentially that the ratio of Al and Fe to inorganic material in the layer beneath the O horizon remains constant once that material is mixed into the O horizon. Our calculations show that top-down deposition is by far the larger source of Al and Fe to the O horizon compared with physical soil mixing, which is consistent with the radionuclide tracer data and the profile chemistry.

When comparing the calculated Al and Fe pools projected for the O horizon from top-down deposition and physical mixing with the measured Al and Fe pools, there are a few different scenarios that emerge (Table 4). At Camels Hump, Mosvik, and Evje, Al and Fe pools calculated from depositional fluxes exceed the observed amounts. These are the three sites that had the longest O horizon turnover times (all >250 years; Table 3), and, it may be that steady-state is rarely attained on this timescale because of episodic events such as tree-throw, forest fires, or other disturbances. Furthermore, we suspect that the calculated Camels Hump deposition flux is too high, probably because the sampled surface layer for the input calculation was too thick (4 cm), resulting in additional Al and Fe levels introduced from sampling beneath the freshest litter that elevated the depositional flux calculation. At Mossilauke and Ducktrap, calculated pools of Al and Fe fall well short of observed pools, and at Amli and Birkenes, calculated pools fall slightly but not always significantly short of observed pools.

Below-ground inputs other than physical soil mixing, possibly a biologically-mediated process, may explain the "missing" Al and Fe here. The O horizon contains organic matter derived from canopy inputs (litterfall), as well as fine roots that come from beneath the surface, but the relative importance of these pools is not well understood. Both litter and root-derived sources can be important fluxes of Fe and Al to the organic soil, and forest composition and structure can have a major impact upon the relative proportion of Fe and Al derived from each. Root-derived Fe and Al represented the most significant flux of these metals to pools of organic detritus in an *Abies amabilis* (Pacific silver fir) stand in the Cascade Mountains, Washington, USA (Vogt et al., 1987). Up to half of the Al fluxes to the O horizon of a *Picea rubens* (Red Spruce) forest in Maine was explained by root activity, but the specific process is unknown (Rustad and Cronan, 1995).

The Maine forests studied by Rustad and Cronan (1995) are similar in parent material and canopy to forests in this study, thus, we would expect both litter and fine roots to be important sources of Fe and Al in this region as well. It is becoming clear that different forest compositions can have a very significant effect on the fluxes and cycling of essential and nonessential elements in the soil profile (e.g., Brandtberg and Simonsson, 2003), and our data suggest that below-ground biological circulation begins to impact the chemistry of aging organic matter after 10 years (Figs. 6 and 7). Li et al. (2008) recently demonstrated that below-ground contributions to the O horizon might be significant for Fe at an aggrading forest on the Southern Piedmont in South Carolina (USA). Through repeated-sampling, they determined that the amount of Fe in the O horizon greatly exceeded that amount that could be explained by atmospheric deposition and above-ground cycling. A number of other recent studies have documented a considerable pool of secondary Al and Fe in O horizon humus (Giesler et al., 2000; Brandtberg and Simonsson, 2003; Li et al., 2008), and some have speculated that this pool of Al and Fe can limit P availability in forests (Giesler et al., 2002). Our dated profile approach provides a unique perspective on how the metal content of decomposing detritus can change with time, and allows us to constrain the timescale and source of metal enrichment in soil organic matter as it decays.

5. CONCLUSIONS

Forest litter decomposition is a complex biogeochemical process regulating the fate of a number of nutrient and contaminant elements in the environment. The conversion of fresh litter into humus takes decades; tracer studies may thus be the only avenue for evaluating the accumulation and loss of elements in decomposing detritus. We use measurements of ^{210}Pb in O horizon layers and in mineral soil to quantify the timescale over which canopy-derived litter is converted into mobile organo-metallic colloids. This production rate varies nearly an order of magnitude across the seven sites studied here, but appears to be slowest at high elevation and high latitude sites, where decomposition rates are presumably the lowest. We dated O horizon layers using a constant flux atmospheric ^{210}Pb model and applied this technique to quantify the accumulation and loss of metals in decomposing forest-derived litter. While layer ages determined by this technique are coarse, in some cases spanning several decades, the dates calculated by the CRS model are consistent with the distribution of independent tracers. Despite their differences in redox chemistry, predicted solubilities, and different biological roles, the fate of Al, Fe, and Pb in the O horizon can be described using a similar model, where these metals are enriched in canopy-derived litter as it decomposes, but are ultimately converted to colloidal phases that are immobilized in the upper mineral soil. The quantities of secondary Al and Fe in the humus layer of the O horizon exceed the levels that can be described by the burial and decomposition of canopy-derived litter. Our data suggest that on short timescales (<100 years), physical mixing of mineral-derived Al and Fe is not a likely mechanism for significantly enriching the O horizon in these metals, and conclude that below- ground biological circulation is a significant process generating secondary Al and Fe in soil humus. In contrast, Mn is rapidly lost from decomposing forest detritus, which may best be explained by a tight cycling of this essential nutrient by the ecosystem or possibly dissolved losses (via leaching). Rapid biological uptake of Mn would limit its transport to the mineral soil, and may explain the lack of accumulated secondary Mn beneath the O horizon we observed here. While

we focused on a limited number of elements in this study, the techniques we use and processes that we quantify may be extended to describe the fate of other nutrients and contaminants in terrestrial environments.

ACKNOWLEDGMENTS

We thank Paul Zietz and Joshua Landis for laboratory assistance, and Burch Fisher for help with the fieldwork at Ducktrap. The first author is grateful to Andrew Schroth and Andrew Quicksall for valuable discussions on the fate of lead and iron in soil environments. We acknowledge the Northeastern States Research Cooperative (USDA Forest Service) for funding to A.J. Friedland, the USDA for funding to B. Bostick and J. Kaste (USDA NRI 2007-03128) and NSF support (EAR-0650533) of Kaste which made this work possible. The authors are grateful to Peter Appleby, S. Krishnaswami, and two anonymous reviewers whose thoughtful comments helped improve our work.

APPENDIX A. SUPPLEMENTARY DATA

Supplementary data associated with this article can be found, in the online version, at doi:10.1016/j.gca.2011.01.011.

REFERENCES

Abadia J. (1991) Leaf responses to Fe deficiency – a review. In *6th International Symp. on Iron*. Marcel Dekker Inc., Logan, UT.

Appleby P. G. (2001) Chronostratigraphic techniques in recent sediments. In *Tracking Environmental Change Using Lake Sediments, Volume 1: Basin Analysis, Coring, and Chronological Techniques* (eds. W. M. Last and J. P. Smol). Kluwer Academic Publishers, Dordrecht.

Appleby P. G. (2008) Three decades of dating recent sediments by fallout radionuclides: a review. *Holocene* **18**, 83–93.

Appleby P. G. and Oldfield F. (1992) Application of lead-210 to sedimentation studies. In *Uranium-series Disequilibrium* (eds. M. Ivanovich and R. S. Harmon). Oxford University Press.

Appleby P. G., Richardson N. and Nolan P. J. (1991) 241Am dating of lake-sediments. *Hydrobiologia* **214**, 35–42.

Artinger R., Schuessler W., Schaefer T. and Kim J. I. (2002) A kinetic study of Am(III)/humic colloid interactions. *Environ. Sci. Technol.* **36**, 4358–4363.

Baker J. P. and Schofield C. L. (1982) Aluminum toxicity to fish in acidic waters. *Water Air Soil Pollut.* **18**, 289–309.

Bargar J. R., Brown G. E. and Parks G. A. (1997a) Surface complexation of Pb(II) at oxide–water interfaces. 1. XAFS and bond-valence determination of mononuclear and polynuclear Pb(II) sorption products on aluminum oxides. *Geochim. Cosmochim. Acta* **61**, 2617–2637.

Bargar J. R., Brown G. E. and Parks G. A. (1997b) Surface complexation of Pb(II) at oxide–water interfaces. 2. XAFS and bond-valence determination of mononuclear Pb(II) sorption products and surface functional groups on iron oxides. *Geochim. Cosmochim. Acta* **61**, 2639–2652.

Baskaran M. (1995) A search for the seasonal variability on the depositional fluxes of Be-7 and Pb-210. *J. Geophys. Res. Atmos.* **100**, 2833–2840.

Berg B. (2000) Litter decomposition and organic matter turnover in northern forest soils. *For. Ecol. Manage.* **133**, 13–22.

Berg T., Royset O. and Steinnes E. (1994) Trace-elements in precipitation at Norwegian background stations (1989–1990) measured by ICP-MS. *Atmos. Environ.* **28**, 3519–3536.

Bjorkvald L., Buffam I., Laudon H. and Morth C. M. (2008) Hydrogeochemistry of Fe and Mn in small boreal streams: the role of seasonality, landscape type and scale. *Geochim. Cosmochim. Acta* **72**, 2789–2804.

Bonniwell E. C., Matisoff G. and Whiting P. J. (1996) Determining the times and distances of particle transit in a mountain stream using fallout radionuclides. In *Association-of-American-Geographers 92nd Annual Meeting*. Elsevier Science Bv, Charlotte, North Carolina.

Bonniwell E. C., Matisoff G. and Whiting P. J. (1999) Determining the times and distances of particle transit in a mountain stream using fallout radionuclides. *Geomorphology* **27**, 75–92.

Brandtberg P. O. and Simonsson M. (2003) Aluminum and iron chemistry in the O horizon changed by a shift in tree species composition. *Biogeochemistry* **63**, 207–228.

Brown L., Stensland G. J., Klein J. and Middleton R. (1989) Atmospheric deposition of Be-7 and Be-10. *Geochim. Cosmochim. Acta* **53**, 135–142.

Brynhildsen L. and Rosswall T. (1997) Effects of metals on the microbial mineralization of organic acids. *Water Air Soil Pollut.* **94**, 45–57.

Bundt M., Albrecht A., Froidevaux P., Blaser P. and Fluhler H. (2000) Impact of preferential flow on radionuclide distribution in soil. *Environ. Sci. Technol.* **34**, 3895–3899.

Cambray R. S., Playford K., Lewis F. N. J. and Carpenter R. C. (1989) Radioactive Fallout in Air and Rain: Results to the End of 1988'. Environ. Med. Sci. Div. Harwell Lab, Oxfordshire.

Chaperon S. and Sauve S. (2007) Toxicity interaction of metals (Ag, Cu, Hg, Zn) to urease and dehydrogenase activities in soils. *Soil Biol. Biochem.* **39**, 2329–2338.

Cloy J. M., Farmer J. G., Graham M. C., MacKenzie A. B. and Cook G. T. (2008) Historical records of atmospheric Pb deposition in four Scottish ombrotrophic peat bogs: an isotopic comparison with other records from western Europe and Greenland. *Global Biogeochem. Cycle* **22**, 16.

Currie W. S. and Aber J. D. (1997) Modeling leaching as a decomposition process in humid Montane forests. *Ecology* **78**, 1844–1860.

Cutshall N. H., Larsen I. L. and Olsen C. R. (1983) Direct analysis of Pb-210 in sediment samples – self-absorption corrections. *Nucl. Instrum. Meth. Phys. Res.* **206**, 309–312.

Davidson E. A. and Janssens I. A. (2006) Temperature sensitivity of soil carbon decomposition and feedbacks to climate change. *Nature* **440**, 165–173.

Dixon J. L., Heimsath A. M., Kaste J. and Amundson R. (2009) Climate-driven processes of hillslope weathering. *Geology* **37**, 975–978.

Donisa C., Steinnes E. and Sjobakk T. E. (2005) Nitric-acid soluble fractions of 21 elements in Norwegian podzols: factors affecting regional differences in vertical distribution. *Appl. Geochem.* **20**, 1258–1267.

Dorr H. and Munnich K. O. (1989) Downward movement of soil organic-matter and its influence on trace-element transport (Pb-210, Cs-137) in the soil. *Radiocarbon* **31**, 655–663.

Dowdall M., Selnaes G., Gwynn J. P. and Davids C. (2004) Simultaneous determination of Ra-226 and U-238 in soil and environmental materials by gamma-spectrometry in the absence of radium progeny equilibrium. *J. Radioanal. Nucl. Chem.* **261**, 513–521.

Drever J. I. (1992) The effect of land plants on weathering rates of silicate minerals. In *Symposium in Honor of Heinrich D Holland*. Pergamon–Elsevier Science Ltd., Reston, VA.

Duce R. A. and Tindale N. W. (1991) Atmospheric transport of iron and its deposition in the ocean. *Limnol. Oceanogr.* **36**, 1715–1726.

Fimmen R. L., Richter D. D., Vasudevan D., Williams M. A. and West L. T. (2008) Rhizogenic Fe–C redox cycling: a hypothetical biogeochemical mechanism that drives crustal weathering in upland soils. *Biogeochemistry* **87**, 127–141.

Galloway J. N., Thornton J. D., Norton S. A., Volchok H. L. and McLean R. A. N. (1982) Trace-metals in atmospheric deposition – a review and assessment. *Atmos. Environ.* **16**, 1677–1700.

Giesler R., Ilvesniemi H., Nyberg L., van Hees P., Starr M., Bishop K., Kareinen T. and Lundstrom U. S. (2000) Distribution and mobilization of Al, Fe and Si in three podzolic soil profiles in relation to the humus layer. *Geoderma* **94**, 249–263.

Giesler R., Petersson T. and Hogberg P. (2002) Phosphorus limitation in boreal forests: effects of aluminum and iron accumulation in the humus layer. *Ecosystems* **5**, 300–314.

Graustein W. C. and Turekian K. K. (1986) 210Pb and 137Cs in air and soils measure the rate and vertical profile of aerosol scavenging. *J. Geophys. Res.* **91**, 14355–14366.

Hawley N., Robbins J. A. and Eadie B. J. (1986) The partitioning of beryllium-7 in fresh water. *Geochim. Cosmochim. Acta* **50**, 1127–1131.

Kaste J. M., Bostick B. C., Friedland A. J., Schroth A. W. and Siccama T. G. (2006a) Fate and speciation of gasoline-derived lead in organic horizons of the northeastern USA. *Soil Sci. Soc. Am. J.* **70**, 1688–1698.

Kaste J. M., Bostick B. C. and Heimsath A. M. (2006b) Determining Th-234 and U-238 in rocks, soils, and sediments via the doublet gamma at 92.5 keV. *Analyst* **131**, 757–763.

Kaste J. M., Friedland A. J. and Miller E. K. (2005) Potentially mobile lead fractions in montane organic-rich soil horizons. *Water Air Soil Pollut.* **167**, 139–154.

Kaste J. M., Friedland A. J. and Sturup S. (2003) Using stable and radioactive isotopes to trace atmospherically deposited Pb in montane forest soils. *Environ. Sci. Technol.* **37**, 3560–3567.

Kaste J. M., Heimsath A. M. and Bostick B. C. (2007) Short-term soil mixing quantified with fallout radionuclides. *Geology* **35**, 243–246.

Kaste J. M., Norton S. A. and Hess C. T. (2002) Environmental Chemistry of Beryllium-7. Beryllium: Mineralogy, Petrology, and Geochemistry. Mineralogical Soc. America, Washington.

Kerndorff H. and Schnitzer M. (1980) Sorption of metals on humic acid. *Geochim. Cosmochim. Acta* **44**, 1701–1708.

Kim G., Hussain N., Church T. M. and Carey W. L. (1997) The fallout isotope Bi-207 in a Delaware salt marsh: a comparison with Pb-210 and Cs-137 as a geochronological tool. *Sci. Total Environ.* **196**, 31–41.

Klaminder J., Bindler R., Emteryd O., Appleby P. and Grip H. (2006) Estimating the mean residence time of lead in the organic horizon of boreal forest soils using 210-lead, stable lead and a soil chronosequence. *Biogeochemistry* **78**, 31–49.

Klaminder J., Bindler R., Rydberg J. and Renberg I. (2008) Is there a chronological record of atmospheric mercury and lead deposition preserved in the mor layer (O-horizon) of boreal forest soils? *Geochim. Cosmochim. Acta* **72**, 703–712.

Klaminder J. and Yoo K. (2008). *Contaminants as Tracers for Studying Dynamics of Soil Formation: Mining an Ocean of Opportunities*. .

Klaminder J., Yoo K. and Giesler R. (2009) Soil carbon accumulation in the dry tundra: important role played by precipitation. *J. Geophys. Res. Biogeosci.* **114**, 9.

Kleber M., Mikutta R., Torn M. S. and Jahn R. (2005) Poorly crystalline mineral phases protect organic matter in acid subsoil horizons. *Eur. J. Soil Sci.* **56**, 717–725.

Krishnaswami S. and Lal D. (1978) Radionuclide limnochrology. In *Lakes, Chemistry, Geology and Physics* (ed. A. Lerman). Springer-Verlag, New York.

Krishnaswami S., Lal D., Martin J. J. and Meybeck M. (1971) Geochronology of lake sediments. *Earth Planet. Sci. Lett.* **11**, 407–414.

Lal D., Malhotra P. K. and Peters B. (1958) On the production of radioisotopes in the atmosphere by comic radiation and their application to meteorology. *J. Atmos. Terr. Phys.* **12**, 306–328.

Li J. W., Richter D. D., Mendoza A. and Heine P. (2008) Four-decade response of soil trace elements to an aggrading old field forest: B, Mn, Zn, Cu, and Fe. *Ecology* **89**, 2911–2923.

Lundstrom U. S., van Breemen N. and Bain D. (2000) The podzolization process. A review. *Geoderma* **94**, 91–107.

Manceau A., Boisset M. C., Sarret G., Hazemann R. L., Mench M., Cambier P. and Prost R. (1996) Direct determination of lead speciation in contaminated soils by EXAFS spectroscopy. *Environ. Sci. Technol.* **30**, 1540–1552.

Miller E. K. and Friedland A. J. (1994) Lead migration in forest soils – response to changing atmospheric inputs. *Environ. Sci. Technol.* **28**, 662–669.

Nozaki Y., Demaster D. J., Lewis D. M. and Turekian K. K. (1978) Atmospheric Pb-210 fluxes determined from soil profiles. *J. Geophys. Res. Oceans Atmos.* **83**, 4047–4051.

Oldfield F., Appleby P. G. and Battarbee R. W. (1978) Alternative 210Pb dating results from the New Guinea Highlands and Lough Erne. *Nature* **271**, 339–342.

Peretyazhko T. and Sposito G. (2005) Iron(III) reduction and phosphorous solubilization in humid tropical forest soils. *Geochim. Cosmochim. Acta* **69**, 3643–3652.

Preiss N., Melieres M. A. and Pourchet M. (1996) A compilation of data on lead 210 concentration in surface air and fluxes at the air–surface and water–sediment interfaces. *J. Geophys. Res. Atmos.* **101**, 28847–28862.

Robbins J. A. (1978) Geochemical and geophysical applications of radioactive lead. In *Biogeochemistry of Lead in the Environment* (ed. J. O. Nriagu). Elsevier Scientific, Amsterdam.

Robbins J. A., Krezoski J. R. and Mozley S. C. (1977) Radioactivity in sediments of the Great Lakes: post-depositional redistribution by deposit-feeding organisms. *Earth Planet. Sci. Lett.* **36**, 325–333.

Russell I. J., Choquette C. E., Fang S. L., Dundulis W. P., Pao A. A. and Pszenny A. A. P. (1981) Forest vegetation as a sink for atmospheric particulates – quantitative studies in rain and dry deposition. *J. Geophys. Res. Oceans Atmos.* **86**, 5247–5363.

Rustad L. E. (1994) Element dynamics along a decay continuum in a red spruce ecosystem in Maine, USA. *Ecology* **75**, 867–879.

Rustad L. E. and Cronan C. S. (1989) Cycling of aluminum and nutrients in litterfall of a Red Spruce (Picea-Rubens Sarg) stand in Maine. *Can. J. For. Res. Rev. Can. Rech. For.* **19**, 18–23.

Rustad L. E. and Cronan C. S. (1995) Biogeochemical controls on aluminum chemistry in the O-horizon of a red spruce (Picea-rubens sarg) stand in central Maine, USA. *Biogeochemistry* **29**, 107–129.

Sauve S., Manna S., Turmel M. C., Roy A. G. and Courchesne F. (2003) Solid–solution partitioning of Cd, Cu, Ni, Pb, and Zn in the organic horizons of a forest soil. *Environ. Sci. Technol.* **37**, 5191–5196.

Sauve S., Martinez C. E., McBride M. and Hendershot W. (2000) Adsorption of free lead (Pb^{2+}) by pedogenic oxides, ferrihydrite, and leaf compost. *Soil Sci. Soc. Am. J.* **64**, 595–599.

Schlesinger W. H. (1977) Carbon balance in terrestrial detritus. *Annu. Rev. Ecol. Syst.* **8**, 51–81.

Schroth A. W., Bostick B. C., Kaste J. M. and Friedland A. J. (2008) Lead sequestration and species redistribution during soil

organic matter decomposition. *Environ. Sci. Technol.* **42**, 3627–3633.

Sheets R. W. and Lawrence A. E. (1999) Temporal dynamics of airborne lead-210 in Missouri (USA): implications for geochronological methods. *Environ. Geol.* **38**, 343–348.

Sherman J., Fernandez I. J., Norton S. A., Ohno T. and Rustad L. E. (2006) Soil aluminum, iron, and phosphorus dynamics in response to long-term experimental nitrogen and sulfur additions at the bear brook watershed in Maine, USA. *Environ. Monit. Assess.* **121**, 421–429.

Shortle W. C. and Smith K. T. (1988) Aluminum-induced calcium deficiency syndrome in declining red spruce. *Science* **240**, 1017–1018.

Shotyk W., Goodsite M. E., Roos-Barraclough F., Frei R., Heinemeier J., Asmund G., Lohse C. and Hansen T. S. (2003) Anthropogenic contributions to atmospheric Hg, Pb and As accumulation recorded by peat cores from southern Greenland and Denmark dated using the 14C "bomb pulse curve". *Geochim. Cosmochim. Acta* **67**, 3991–4011.

Steinnes E., Sjobakk T. E., Donisa C. and Brannvall M. L. (2005) Quantification of pollutant lead in forest soils'. *Soil Sci. Soc. Am. J.* **69**, 1399–1404.

Vogt K. A., Dahlgren R., Ugolini F., Zabowski D., Moore E. E. and Zasoski R. (1987) Aluminum, Fe, Ca, Mg, K, Mn, Cu, Zn, and P in aboveground and belowground biomass 2. Pools and circulation in a sub-alpine Abies-Amabilis stand. *Biogeochemistry* **4**, 295–311.

Wallbrink P. J. and Murray A. S. (1996) Distribution and variability of Be-7 in soils under different surface cover conditions and its potential for describing soil redistribution processes. *Water Resour. Res.* **32**, 467–476.

Wallbrink P. J., Murray A. S. and Olley J. M. (1999) Relating suspended sediment to its original soil depth using fallout radionuclides. *Soil Sci. Soc. Am. J.* **63**, 369–378.

Wang E. X. and Benoit G. (1997) Fate and transport of contaminant lead in spodosols: a simple box model analysis. *Water Air Soil Pollut.* **95**, 381–397.

Wang E. X., Bormann F. H. and Benoit G. (1995) Evidence of complete retention of atmospheric lead in the soils of Northern Hardwood forested ecosystems. *Environ. Sci. Technol.* **29**, 735–739.

Wiederhold J. G., Teutsch N., Kraemer S. M., Halliday A. N. and Kretzschmar R. (2007) Iron isotope fractionation in oxic soils by mineral weathering and podzolization. *Geochim. Cosmochim. Acta* **71**, 5821–5833.

You C. F., Lee T. and Li Y. H. (1989) The partition of Be between soil and water. *Chem. Geol.* **77**, 105–118.

Associate editor: S. Krishnaswami